Romain JAN
romain.jan@isae-supaero.fr

Experimental validation of ASWING. Part IV: Aeroelasticity

Supervisors:
- Prof J-M. Moschetta
- Prof J-P. Condomines

Abstract

This technical report deals with the fourth and last part of the experimental evaluation and modification of ASWING. It focuses on the aeroelastic features of the software. Experimental data from the literature have been gathered to evaluate the good prediction of deflections and twists under steady flow and their effect on aerodynamic control surfaces effectiveness. Based on that last case, modifications of the code are proposed to provide better flap/aileron rolling performance predictions. Then, the predictions of torsional and flutter divergence are discussed. The impact of different parameters such as the angle of attack and the position of a nacelle on the latter are discussed. Whirl flutter on a propeller/wing configuration closes the part on dynamic phenomena. The report continues with a discussion on the response of a flexible aircraft to a vertical gust and the post-flutter limit cycle oscillations. Finally, the impact of folding wingtip devices on gust alleviation and rolling performances is discussed.

Important note to the reader:
This work has not been peer reviewed yet. Only the author's PhD referee members (Professors Mark Drela, Rafael Palacios, Eric Laurendeau and Murat Bronz) had access to this work and have authorised the defence.For more details, please refers to https://www.theses.fr/s251420. Nevertheless, this material is in a process of publication in peer reviewed journals, in a shorter version. This document will be updated if new material has to be added.

About the data presented in this report:
This report presents various comparisons with different sets of experimental data. The latter and numerical simulations are available on demand. However, if you consider using them for your own studies, please cite this work and the related ones from which data are coming. Contact: romain.jan@isae-supaero.fr

Version notes

This technical report aims to be updated if new experimental cases and ASWING modifications have to be added. Also, the updates aim to take into account the feedback of the community (typos, theoretical development mistakes, etc).
Versioning syntax:
The version of this document is given as follows: IV.X.y, where IV denotes the fourth part of this experimental evaluation, X and y denote respectively major and minor updates.

- **Version IV.1.0:**
  (30/07/2023) This version is the one submitted to the author's PhD referee as a partial fulfilment of the PhD degree. This version presented the following experimental cases:

    - Some low aspect ratio wings with various composite layouts have been used to assess the tip deflections and twists under steady flow. The flutter speeds and frequencies at various angles of attack are also discussed. Divergence speed prediction is also assessed. Finally, limit cycle oscillations on this bench are discussed.

    - A trapezoidal wing with various aileron configurations is used to assess the control surfaces loss of effectiveness up to reversal speed.

    - A straight wing with concentrated weight anchored to it is used to assess the effect of a nacelle position on the flutter speed and frequency.

    - Two last benches presenting folding wingtips are used to assess their effect on gust alleviation and rolling performances.

- **Version IV.2.0:**
  (16/01/2024) Major typos have been corrected. Some experimental validation cases have been added and are summed up as follows:

    - The Pazy wing bench (moderate aspect ratio) has been used to assess tip deflections and twists under steady flow. It has also been used to quantify the prediction quality of ASWING of the flutter boundaries (speed and frequency).

- **Version IV.3.0:**
  (13/07/2024) The document has been rearranged to fit the other report formalism.

    - Aeroelastic cases have been renamed $\mathcal{AE} - 1 - 7$ to match the other technical report formalism

    - A new flared folding wing tip case has been added, where the effect of zero non-side slip angle is considered.

    - A subsection has been added to propose a discussion on the Aswing prediction of the effect of tailerons in light of the evaluation cases presented in this work.

    - A subsection has been added to propose a discussion on transonic flutter prediction limitations and to propose a future modification of the code in order to solve it.

    - A new flared folding wingtip case has been added, where the effect of the flare and the wingtip flap angles on the flutter onset are considered.

    - A new flared folding wing tip case has been added, where the effect of the flare angle on the gust alleviation performance is qualitatively discussed.

    - Names of this PhD program supervisors have been added to this document.

    - Names of this PhD referee members have been added to the note to the reader.

Contents

1   Introduction

Ith the increasing need for aircraft to minimize their carbon footprint, the first vector of aerodynamic performance improvements is the increase of the wingspan. Indeed, this tends to reduce the vorticity of the wing tips inducing the lift-induced drag (accounting for the biggest contribution to drag). Or a higher aspect ratio geometry is generally more flexible, thus raising new issues. Those aircraft are therefore much more likely to encounter aeroelastic phenomena in their flight envelope. Among them, torsional divergences and flutter, reduction of the aerodynamic control surfaces effectiveness up to the reversal behaviour can be mentionned. In addition, the position of a nacelle or an external tank on a wing can drastically change its aeroelastic response. In the same way, a rotating propeller, or an inertial defect of a rotating machine (engine, turbofan etc) can lead to a premature flutter of the structure. All these phenomena are of first order from an aeronautical safety point of view and define the upper bound of the aircraft flight envelope. They are generally defined by critical speeds (flutter, divergence and control reversal speed). In this sense, having a rapid diagnostic and analysis tool that allows the accurate prediction of these phenomena is essential in the modern aircraft design chain. The recent Aura Aero crash (BEA report n C-2022-06-A) caused by flutter during a high load factor manoeuvre, unfortunately, recalls the need for such predesign tool.

Other aeroelastic phenomena of interest can be mentioned, such as deformation and twist under steady flow, which provide interesting insight on the aerodynamic performance of a wing once deformed at different flight conditions. The local modification of the twist can also give information on the stall and the ailerons unusability (washout). Again from an aeronautical safety point of view, the intensity of turbulence and gusts encountered during flights is likely to increase due to climate change. In this sense, having a tool that can predict the aeroelastic response of an aircraft to a gust or turbulence is a real asset. In particular, the root bending moment time response is often of interest in terms of structural failure forecast. Moreover some more fundamental phenomena can be of interest, such as post-flutter limit cycle oscillations. Another issue arise by airline companies is the use of folding wingtip to reduce airport taxes rising with the aircraft span. It turns out that those devices can bring benefits to the behaviour of the aircraft in flight Castrichini et al. (2016 and 2017), Cheung et al. (2017, 2018, 2020 and 2022) and Healy et al. (2022c, 2022b, 2022d and 2022a). Having a tool allowing the fast study of those devices is also of interest to an aircraft manufacturer.

ASWING integrates and proposes the study of all the phenomena mentioned above. As a consequence, this technical report is the fourth and last part of an experimental evaluation work of ASWING. This one focuses on the evaluation of the prediction quality of the aeroelastic phenomena mentioned earlier.

2   Experimental evaluation

This section shortly presents the evaluation methodology of the aeroelastic features of ASWING. It focuses first on aeroelasticity phenomena. The steady phenomena are addressed first with the wing deflection and twist as well as ailerons/flap effectiveness under steady flow. Then comes the phenomena involving the dynamics of the structure, namely flutter, torsional divergence, whirl flutter, the impact of the angle of attack and the position of a nacelle on these. The aeroelastic part ends with the unsteady phenomena prediction evaluation namely, the response to a gust and the post-flutter limit cycle oscillations. In a second time, the folding wing tip devices are studied, in particular their impact on the rolling performances, the flutter onset and their ability to effectively alleviate a gust. As for the previous evaluation part, the experimental cases have been chosen as stressful as possible for the theoretical model. Most of the cases present then low aspect ratio wings. They are presented in table 1

3   Aeroelastic features:

This section presents the 7 aeroelastic evaluation cases. Each cases has been carefully chosen to stress a specific feature of Aswing. Then a short section are dedicated to non evaluated features invoking works from the literature. Some discussions on some are proposed in light of the cases presented, as some conclusions can be drawn by mixing them.

3.1   Case AE-1-Steady : tip deflection and twist of a moderate aspect ratio straight wing

The first feature to be evaluated is the steady tip deflection and twist predictions. The latters are of interest in the design of an aircraft as they provide relevant intel. For example, capturing them correctly can give an insight on their consequences on aerodynamic performances such as lift-to-drag ratio. The total lift stall being of interest to define the flight

Table 1: Experimental evaluation cases. $\mathcal{AE} = \mathcal{A}$ero $\mathcal{E}$lasticity. $\mathcal{S} = \mathcal{S}$teady, $\mathcal{D} = \mathcal{D}$ynamic and $\mathcal{U} = \mathcal{U}$nsteady. $\mathcal{FFWT} = \mathcal{F}$lared $\mathcal{F}$olding $\mathcal{W}$ing $\mathcal{T}$ips

CASE	Geometry	Exp data	Evaluation type
$\mathcal{AE}$-**1**-$\mathcal{S}$	Straight wing of moderate aspect ratio (Pazy Wing)	[1]	Tip twist and deflection under steady flow at various speed and angle of attack
$\mathcal{AE}$-**2**-$\mathcal{S}$	3 Straight wing of low aspect ratio with various composite layouts	[15, 16]	Tip twist and deflection under steady flow at various speed and angle of attack. Effect of bending torsion coupling
$\mathcal{AE}$-**3**-$\mathcal{S}$	Trapezoidal wing of moderate aspect ratio with various ailerons configuration	[10]	Ailerons loss of effectiveness and reversal speed
$\mathcal{AE}$-**4**-$\mathcal{D}$	Straight wing of moderate aspect ratio (Pazy Wing)	[12]	Flutter boundaries and divergence speed.
$\mathcal{AE}$-**5**-$\mathcal{D}$	3 Straight wing of low aspect ratio with various composite layouts	[15, 16]	Flutter boundaries and divergence speed.
$\mathcal{AE}$-**6**-$\mathcal{D}$	Straight wing of moderate aspect ratio.	[33]	Effect of a tank/nacelle lateral/longitudinal position on the flutter onset.
$\mathcal{AE}$-**7**-$\mathcal{U}$	3 Straight wing of low aspect ratio with various composite layouts	[15, 16]	Limit Cycle Oscillations amplitude variation above the flutter speed.
$\mathcal{FFWT}$-**1**-$\mathcal{S}$	Straight wing with 3 Flared angles	[18]	Lateral and Longitudinal behavior of 3 Flared Folding Wing Tips
$\mathcal{FFWT}$-**2**-$\mathcal{D}$	Straight wing with 2 Flared angles	[22]	Effect of Flared Folding Wing Tips on rolling performance.
$\mathcal{FFWT}$-**3**-$\mathcal{U}$	Swept back wing	[4]	Gust alleviation performance with and without Flared Folding Wing Tips
$\mathcal{FFWT}$-**4**-$\mathcal{U}$	Straight wing with 3 Flared angles	[18]	Gust alleviation performance with and without Flared Folding Wing Tips.
$\mathcal{FFWT}$**5**-$\mathcal{U}$	Straight wing with 2 Flared angles	[21]	Effect of flare and tab angles on the flutter onset.

envelope lower bound can be predicted. Secondly, it is possible for a given flight speed and angle of attack to evaluate the maximum extensional and shear strains locally on the structure implied by the aerodynamic loads. Fibres strain computation can provide insight into when structural failure will occur. Sometimes before the flutter and divergence phenomenon. Finally lifting surface washout can be investigated with this feature. The local stall can be computed and structural modification can be implemented to optimize its appearance and spanwise position so that, the local section where the control surfaces are (flap, ailerons) do not stall first. To evaluate this feature, two experimental benches have been used that are a low and moderate aspect ratio straight wing. The work of Dunn 1992 (presented to the community in Dunn and Dugundji 1992) has been used for the low aspect ratio wing. Note that the experimental bench presented in the latter is used to evaluate other features which are: flutter and divergence speed, flutter boundaries and limit cycle oscillations. For the moderate aspect ratio, a more modern data set from Avin et al. (2022) has been used.

Experimental bench:
The steady tip and twist deflection is refined with the experimental bench of Avin et al. (2022) denoted as Pazy. The wing is straight with an aspect ratio of 5.5. The structure is made of a flat aluminium plate. The latter is wrapped with a series of plastic ribs and and shell to recover the shape of a NACA0018. The wing was placed in the Technion low-speed wind tunnel. Tip displacement and twist were measured at various speed and angle of attack. For more details on the measurement devices please refer to the author's work.

Numerical bench:
The Pazy wing bench was reproduced in ASWING using the structural parameters provided by Riso and Cesnik (2023). A numerical sensor was placed at the tip of the wing around the mid-chord.

Results:
Figures 1 (a) to (d) present the ASWING prediction against Avin et al.'s experimental measurements. Figures 1 (a) and (b) present the tip displacement and twist against airspeed for a root angle of attack of $\alpha = 5°$ while figure 1 (c) and (d) present the tip displacement and twist against airspeed for a root angle of attack of $\alpha = 7°$. For tip deflection, ASWING shows good agreement with the experiment until large amplitude. For $\alpha = 5°$ predictions are weaker. For tip twist, the prediction errors vary quite a lot mostly due to the difficulty of Avin et al. to measure it. Nevertheless, predictions are satisfactory. Finally, the ASWING predictions have been compared to the ones of UM/NAST provided by Riso and Cesnik (2023). As it can be seen similar results are obtained. The UM/NAST more sophisticated structural model does

not show any better performances than ASWING except at very large amplitude when $\alpha = 5°$. In conclusion, ASWING is able to capture correclty the steady aeroelastic behaviour of the Pazy wing

3.2   Case AE-2-Steady : tip deflection and twist of a low aspect ratio composite straight wing

Experimental bench:
The wing is made of a flat 6-plies composite plate with styrofoam fairings glued to it, to reproduce a NACA0012 shape. In total 3 wings were built with 3 different composite layouts involving different stiffness coupling. The latter has been adapted to the ASWING formalism and derived in Table 10. Each wing aspect ratio was 4 making them excellent stress cases for the ASWING model. Each wing was cantilevered to a rotating aluminium clamping device as depicted in figure 2. The latter playing also the role of a plane of symmetry. It was reported by the author that the foam pieces were contributing a lot to the torsion stiffness, the elastic and tension axis was reported to lie on the 0.4 and 0.35 chord lines. The tests were performed in the MIT Department of Aeronautics and Astronautics Acoustics open throat 1.5 by 2.3 meters wind tunnel. The speed range was varying from 0 to 30 m/s. The level of turbulence in the wind tunnel was not reported. For each wing, the tip deflections and twist measurements were captured for 4 different angles of attack ($\alpha = 1$, 5, 10, and 15°) on the speed range until divergence or flutter occurs. Near those phenomena, experimental data was reported to become difficult to track. Higher error bars appear in consequence on the further plots. Among the composite layouts, an uncouple one ($[0_3/90]_S$)[1] was presented as a baseline case while 2 others were presenting positive and negative torsion/bending coupling ($[+15_2/0_2]_S$ and $[-15_2/0_2]_S$).

Numerical bench:
In ASWING, each bench has been reproduced with the laminates properties of table 10. As the wing was anchored vertically to a symmetry plane, the ground flag for the solid surface was activated (see *section 4.5* of Drela-2009). Two numerical sensors were placed at the wing tip, at the leading and trailing edge. Both were capturing the tip deflection. The geometric tip twist was directly provided by ASWING OPER Menu. Forty circulations and 40 structural node variables clustered with a cosine function were enough to ensure converged predictions. An XFOIL analysis of the

---

[1]This notations means that the composite beam is made of sandwich of different fibers with various orientation. Their orientation are defined relatively to the spanwise axis.

(a) $\alpha = 5°$ tip delfection

(b) $\alpha = 5°$ tip twist

(c) $\alpha = 7°$ tip delfection
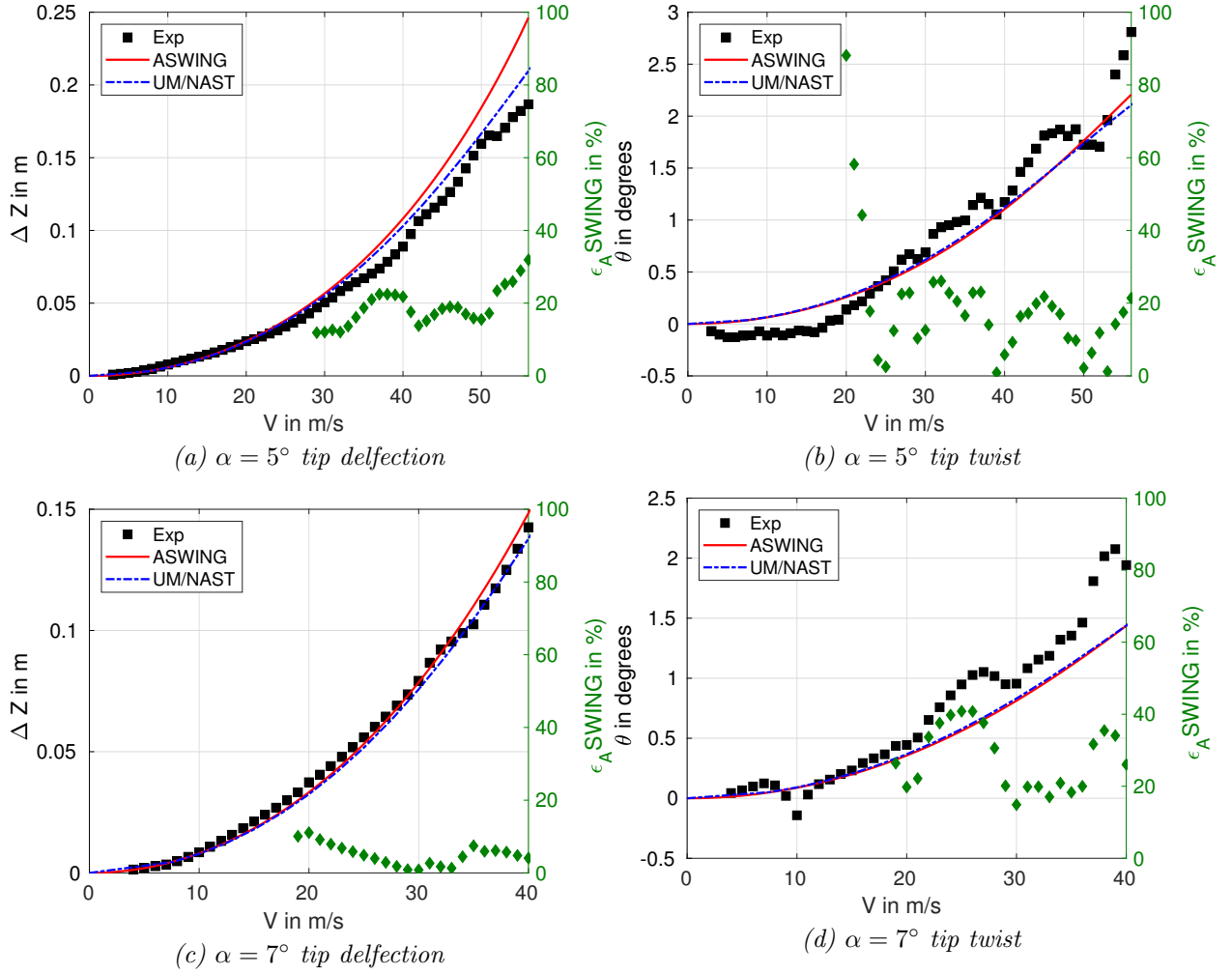
(d) $\alpha = 7°$ tip twist

Figure 1: Case $\mathcal{AE} - 1$: Pazy wing, tip deflection and twist at various angle of attack. ASWING and UM/NAST (Riso and Cesnik-2023) UMNAST predictions comparison with experiments Avin et al.-2022

NACA0012 at the corresponding Reynolds number has been fulfilled leading to the retain parameters $c_{l,\alpha} = 5.73$, $c_{l,min} = -1.1$ and $c_{l,max} = 1.1$. The drag polar were neglected as assumed to have a very small impact on the structural deformations.

Results:
Figure 3 (a) to (f) present a comparison between ASWING predictions and Dunn and Dugundji's experimental data (1992 and 1992) for each laminate considered in his work. The same x and y axis scales have been used for all the figures to clearly highlight the benefit or not of the layouts.

For the $[0_3/90]_S$ layout, (figure 3 a and b) ASWING seems to capture quite well the tip deflection and twist for moderate speed. Near maximum ones, it tends to underestimate the twist. Moreover, at high angle of attack ($\alpha = 10°$ and $15°$), the tip deflections are overestimated no matter the speed. ASWING has an embedded stall function (see *section 5.7* Drela- 2009 documentation), however, it only damps the linear lift slope after the stall occurs. It can not catch the lift drop and slightly overestimates it so the discrepancies on the tip deflections.

For the $[+15_2/0_2]_S$ layout (figure 3 c and d), the predictions are in excellent agreement with experiments no matter the speed or the angle of attack. ASWING clearly captures the effects and benefits of a positive bending torsion coupling stiffness. The structure tends to reduce the tip angle of attack. This in effect will lead the wing tip to stall much later reducing the ASWING prediction discrepancies.

For the $[-15_2/0_2]_S$ layout (figure 3 e and f), because of the negative bending torsion coupling stiffness, the structure tends to rise the wing tip angle of attack as depicted on figure 3 (f), this local stall occurs very quickly even at low root angle of attack. ASWING looses rapidly the track with experiments but clearly capture the tendency imposed by the composite tailoring.

Overall, ASWING shows good agreements with Dunn's steady tip deflections and twist measurements (1992). It becomes weaker at high angle of attack $\alpha = 15°$ (post-stall). More importantly, it captures well the structure tailoring impact which is mandatory in the case of an aircraft design. Last comments must be made on those results. The maximum tip deflection witnessed was around 0.3m ie 55% of the wing span. This can be nearly considered as high deflections. Or in the structural part of this evaluation work (Part III), huge discrepancies were witnessed for static tip load deflections. For the maximum applied mass, the tip deflection was not exceeding 30% or the span. It seems from the aero-elastic evaluation that the tip load test is very conservative. In reality, the aerodynamic lift being quasi elliptically distributed along the span, induced structural loads much more smoothly

scattered. The structural model is thus less sensitive to high tip load leading to less discrepancies. In consequence, tip load deflection tests are not the most appropriate for aero-elastic code separate evaluation as they overestimate the real loads that could be applied on a wing.

3.3   Case AE-3-Steady : ailerons effectiveness and reversal speed of a trapezoidal wing

Aerodynamic control surfaces (ailerons, flaps etc) can be implemented in ASWING. The latter, when deflected modify the lift and pitch moment locally, deforming, in consequence, the structure. This change in the wing or aircraft shape can drastically impact the flap/aileron effectiveness up to a point where reverse behaviour is witnessed. The latter is mentioned in the literature as reversal speed. An inverse behaviour is not necessarily dangerous a priori as long as its appearance is known. However, usually, the reversal speed is very close to aeroelastic divergence phenomenom such as flutter and divergence. For a pilot, all those 3 phenomena set an upper bound limit to the flight envelope not to be exceeded. In consequence, the experimental study of Cole (1951) has been used to evaluate ASWING on this feature. The authors investigated the rolling moments and free rolling rate due to aileron deflection for various speed and flap geometries.

Experimental bench:
Investigations were done on 2 different wings : a straight and swept back wing. In this work, only the straight wing will be considered as reported as the worst case. The tests were performed in the F.K Kirsten wind tunnel with an 8 by 12 feet (2.4 by 3.7 meters) test section. The wing considered was straight and tapered. Its span, taper ratio and aspect ratio were respectively $b = 4ft$ (1.2m), $\lambda = 0.45$, $AR = 8$. The airfoil section was a NACA 63A012. The wing geometry is depicted in figure 9. Several ailerons size were tested. The hinge position was always fixed at 70% of the chord from the leading edge. However, the flap spanwise length could vary in the next interval 0.2, 0.4, 0.6, 0.8 and 0.95 the half span.During the tests, 2 mounts were considered.
Mount 1: the wing is attached to a balance and cannot roll. For several wind speeds the flaps were deflected and the roll moment C_l was measured with a balance and reported. Results were presented as the roll moment induced by a deflected flap $\frac{\partial C_l}{\partial \delta F}$.
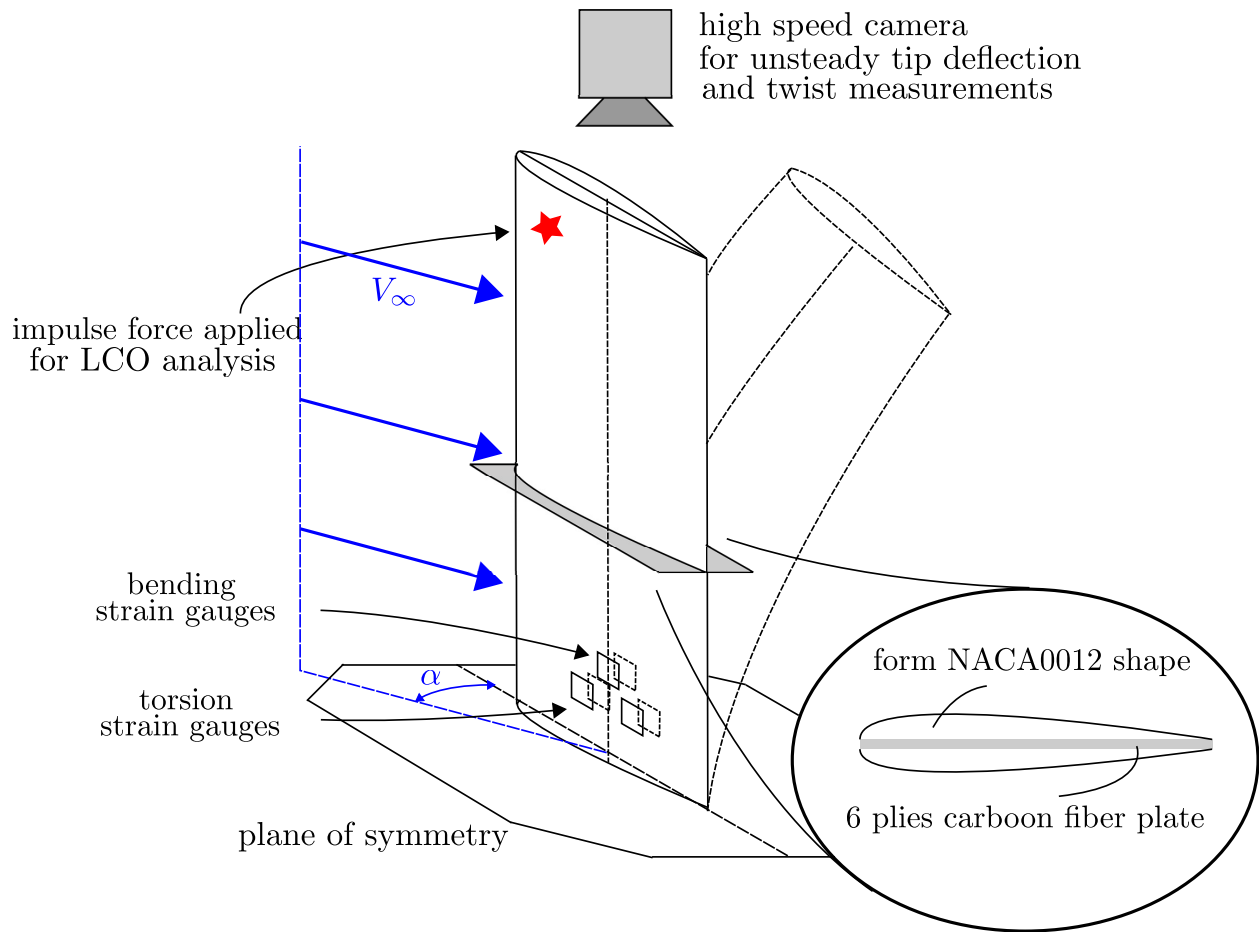**Mount 2:** The wing was free to roll. Over the same

Figure 2: Case $\mathcal{AE} - 2$: :Steady tip deflection and twist, flutter and divergence speed, limit cycle oscillations Dunn's experimental bench (1992)
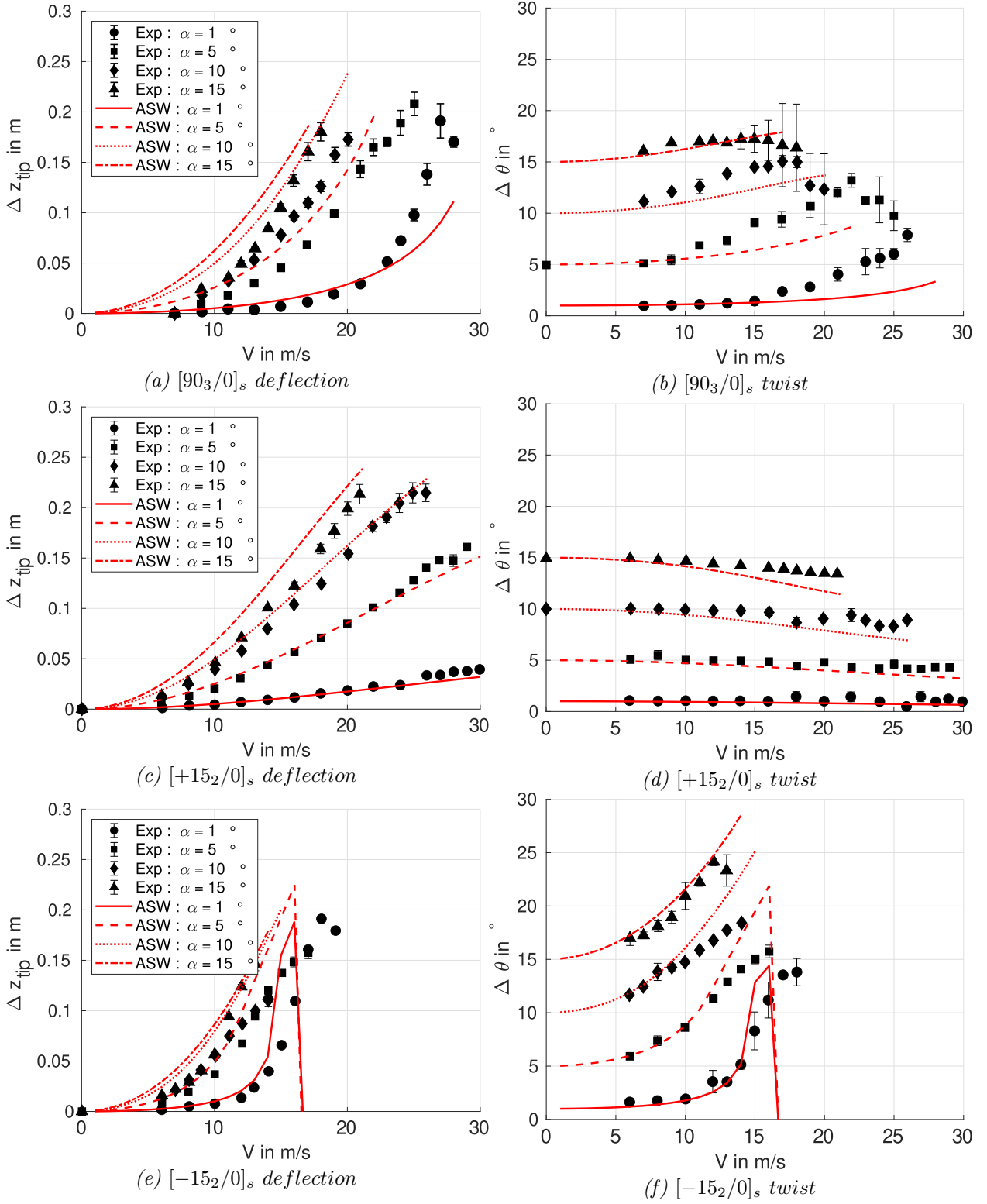
Figure 3: Case $\mathcal{AE} - 2$: Time average tip deflection and twist in function of the flight speed and angle of attack. ASWING 5.96 predictions comparison with experimental data Dunn (1992)

speed range, the rolling rate has been measured for every flap configuration. The author presented the results as the helix angle induced by a flap deflection $\frac{\partial pb/2V}{\partial \delta F}$ against the dynamic pressure q_∞. The helix angle is represented on the right side of the figure 9. Note that p is the wing rolling rate. The latter data is presented in this way as it has been reported by the authors to vary linearly with the dynamic pressure. It is also much more convenient for prediction comparisons. Finally, the authors experienced flutter earlier for configuration with larger flaps so the number of measurements decreases with the flap length increasing.

Numerical bench:
Numerically, the NACA63A012 2D polars were computed with XFOIL. As the speed in the experiments were varying, the analysis was performed over the equivalent range of Reynolds number (Re = 300-600E3). Then $\alpha_0 = 0.0°$, $cl_\alpha = 5.66$, $\partial c_l/\partial \delta F = 0.0581$, $\partial c_{m,0}/\partial \delta F = -0.0107$ were used. A benefit of this evaluation case is to introduce an ASWING modification. An inner function has been implemented to take into account the Reynolds number effect on the flap and airfoil polars directly in the loop. At each chordwize location, a local Reynolds number is computed, then the flap derivatives is interpolated accordingly thanks to a lookup table. The latter provides the variation of flap derivatives with the Reynolds number. Here only 2 points have been used. For elliptical wings, where the Reynolds can reach 0 towards the tip, the flap derivatives is clipped to lower value of the look-up table. This modification is denoted as ASWING-m. This change was motivated by the important variation of $\partial c_l/\partial \delta F$ and $\partial c_{m,0}/\partial \delta F$ on the speed range ie (16% and 5%). Note that for ASWING 5.96 constant values taken at the highest Reynolds number were used as the main objective was to find the reversal speed. ASWING-m was fed with the polars computed from the XFOIL analysis. The torsional and bending stiffness of the wing varies cubically with the spanwise coordinate so they can not be provided here. Please refer to *figure 10* of Cole (1951) for their values. Unfortunately, the mass and inertia distribution were not provided in the document so rolling accelerations could not be compared with the experimental data.

Results:
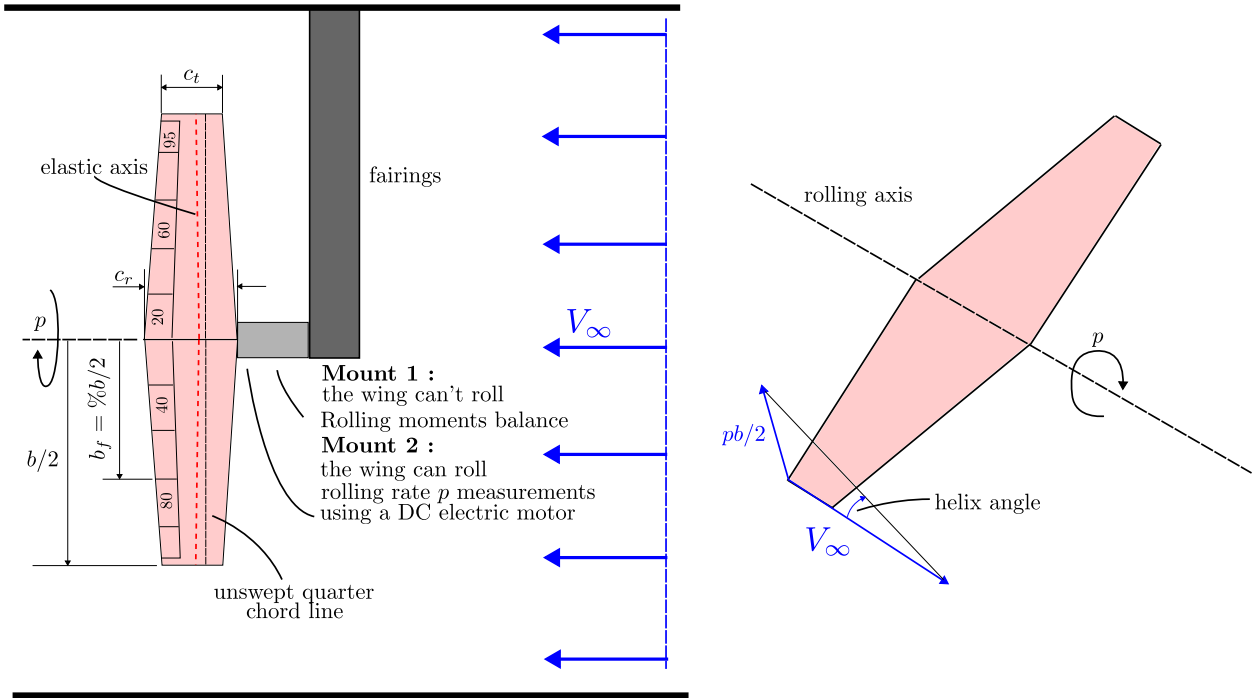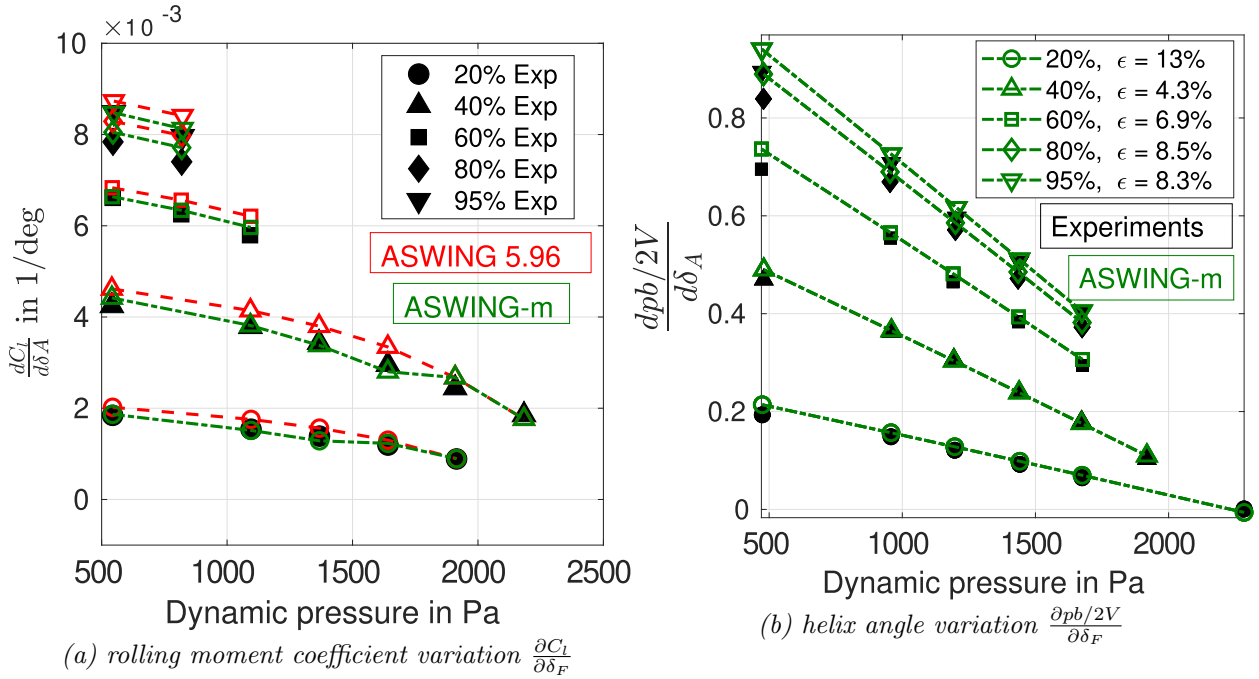ASWING 5.96 and ASWING-m predictions for $\frac{\partial Cl}{\partial \delta F}$ are presented against experimental measurements on the figure 5(a). The advantage of taking into account the variation of the aerodynamic parameters with the Reynolds number is clearly highlighted by the green lines. Predictions tend to be equivalent with the dynamic pressure rising. For the sake of clarity, only ASWING-m $\frac{\partial pb/2V}{\partial \delta F}$ predictions are presented on figure 5(b). Linear slopes were computed and compared to the experiment's. ASWING-m shows good agree-

ment with the experiments no matter the size of the ailerons, with a mean slope error below 8%. Note that ASWING 5.96 was not that far with a 12% error. The reversal speed can be identified from the helix angle plots when the latter crosses the 0.0 y-axes. Prediction errors were in the same range as the slope's. Note that the modification is not a breakthrough improvement, but it does bring comfort of use, avoiding computing aerodynamic parameters for each condition that has be investigated. The aerodynamic polars must be generated only once on the first-guess flight envelope (large enough). Thus ASWING 5.96 ASWING-m can be used to predict the flaps effectiveness and their reversal speed.

3.4 Case AE-4-Dynamic: flutter boundaries and divergence speed of the Pazy wing

Dunn and Dugundji also studied the impact of wing incidence on wing flutter appearance. Figure 6 shows the variation of the flutter or divergence speed with the angle of attack. The predictions of ASWING and Dunn's model are compared to the experimental data of the same author. Note that the ASWING predictions did not all converge especially on the $[0_3/90]_S$ and $[-15_2/0_2]_S$ laminates. Indeed, a bounce was identified of the flutter modes against the imaginary axis probably due to a stiffening of the structure in the ASWING structural model for high amplitude deflections. Obviously, that stiffening is not consistent with the experimental observations. As we have seen, the layout $[+15_2/0_2]_S$ tends to delay high amplitudes of deflection, so the same phenomena have not been witnessed, and the flutter speed could be computed on the considered angle of attack range. On the three layouts considered, for low angle of attack, ASWING captures well the flutter speed decrease and has similar predictions quality as Dunn and Dugundji's model. For the $[0_3/90]_S$, ASWING and Dunn and Dugundji's finite element model present similar predictions and can be considered as consistent with experiments until $\alpha = 10°$ which is the stall angle of attack. After that value, both models are weak to predict the flutter. Thus for the flutter boundaries analysis, higher aspect ratio geometries are recommended in light of the non-satisfying results.

As Dunn and Dugundji's bench is quite stressful for the theoretical model (low aspect ratio), The Pazy wing bench from Drachinsky et al. (2022) has been used to see if ASWING is able to capture the flutter boundaries of a moderate aspect ratio wing. Regarding the bench, a rectangular straight wing of an aspect ratio 5.5 has been placed in the Technion

Figure 4: Case $\mathcal{AE}-3$ Experimental bench of Cole (1951)

(a) rolling moment coefficient variation $\frac{\partial C_l}{\partial \delta_F}$

(b) helix angle variation $\frac{\partial pb/2V}{\partial \delta_F}$

Figure 5: Case $\mathcal{AE}-3$ Ailerons effectiveness and reversal speed predictions. Comparison with experiments from Cole (1951)
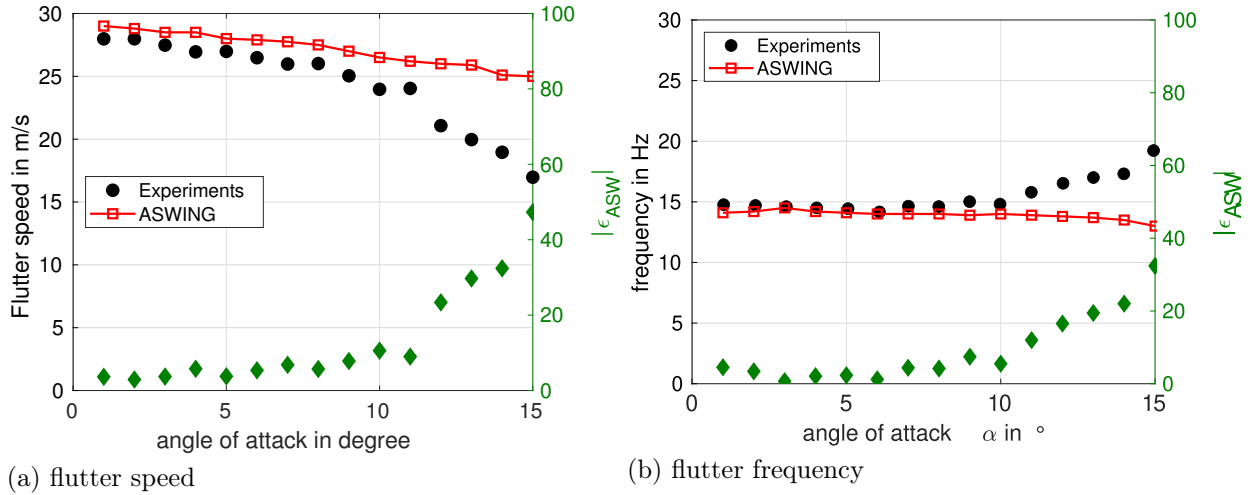
(a) flutter speed

(b) flutter frequency

Figure 6: Case $\mathcal{AE} - 5$: Flutter boundaries of the $[+15_2/0_2]_s$ layout. ASWING predictions against experimental data of Dunn and Dugundji-1992

low Reynolds number wind tunnel. It was mounted vertically (denoted as unload case) and horizontally with a plane of symmetry (loaded case). The angle of attack of the wing was fixed at various values, then the wind tunnel speed varied until flutter was reached. The tests were testing sweep up and down of the speed to detect the flutter zone of the Pazy wing and so at each angle of attack. The flutter zone is highlighted in figure 7 (a) by the green colour. For more details about the bench, the reader is invited to take a deeper look at Drachinsky et al.'s work. In consequence, the bench was reproduced numerically with ease. The Pazy wing equivalent beam model parameters can be found in the work of Riso and Cesnik (2023). Figure 7 (a) presents the ASWING flutter and divergence speed prediction against the experimental data from Drachinsky et al.. From it, ASWING captures well the flutter boundaries no matter the angle of attack of the wing. Table 2 presents a more detailed analysis of those results, and compares the ASWING predictions with the one of UM/NAST performed by Riso and Cesnik (2023). From it, ASWING has the same prediction difference as UM/NAST despite its less sophisticated beam model. The aspect ratio of the wing is high enough to make the Euler-Bernoulli beam model of ASWING relevant in this case. The same conclusion can be drawn from table 3 for the flutter frequency. No matter the case the ASWING prediction errors are below 7%. The unloaded case flutter and divergence speed predictions are compared to the work of Riso and Cesnik (2023) where the reference data is denoted as SOL 145. Again ASWING shows good agreement with the higher fidelity data with a prediction error below 6% (very close to UM/NAST performances).

For the Pazy wing, ASWING shows good predictions of the flutter speed and frequency as well as the divergence. However Drachinsky et al. specified that the

Pazy wing once entered a flutter regime was not diverging and was even going to a stable state after the speed raised enough. Or from the ASWING modal analysis depicted in figure 7 (b), the Pazy wing is supposed to diverge between the flutter boundaries as the flutter mode damping ratio is negative. To make sure that ASWING is able to capture this self-oscillatory behaviour (Limit cycle Oscillations), a complete time marching computation of the wing has to be performed. The initial speed of the wing was set up in the flutter boundary, then a small impulsive perturbation was applied (flap deflection). The simulations were run over a significant amount of flutter period to make sure the wing is really in LCO behaviour. Figures 7 (c) and (d) present those simulations for $\alpha = 3°$ and $\alpha = 5°$. From them, ASWING predicts that the Pazy wing is indeed in a limit cycle oscillation behaviour between the flutter boundaries and so on each angle of attack. This statement must be clarified. Indeed Drachinsky et al. observed that depending on if the speed was going up or down, the Pazy wing was leaving the LCO regime at a different speed than the one predicted by the modal analysis. In other words, ASWING predicts well the lower flutter boundary if the speed is going up and caputure well the upper one if it's slowing down. However if the speed is going up, the Pazy wing leaves its LCO regime later than the modal prediction predictions. It means that the LCO involves a non-linear phenomenon that is not captured by ASWING. Our first guess would be the leading edge vortices that can appear in plunging and pitching motion as reported by (Chiereghin et al. 2017). The leading edge vortices can take some time to vanish and represent a source of exogenous input keeping the overall system self exited for a while until the structural and linear aerodynamic damping effects become stronger.
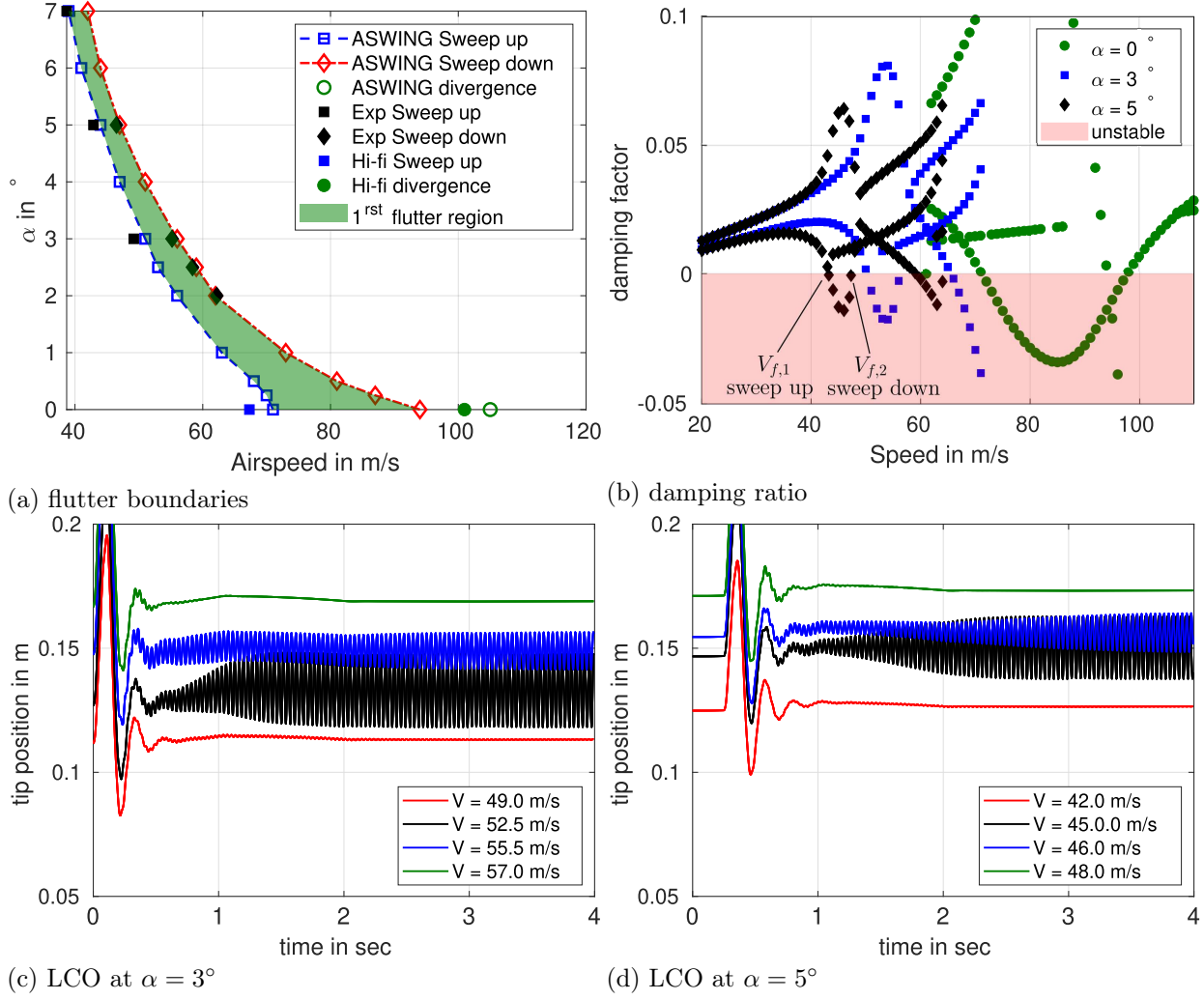
(a) flutter boundaries

(b) damping ratio

(c) LCO at $\alpha = 3°$

(d) LCO at $\alpha = 5°$

Figure 7: Case $\mathcal{AE} - 4$: Pazy wing, flutter boundaries ASWING predictions agaits experiments Drachinsky et al.-2022

Flutter onset						
α (in deg)	Sweep type	Exp.	UM/NAST	ϵ_U (%)	ASWING	ϵ_A (%)
3	Up	49,00	48,24	-1,55	51	4,08
5	Up	43,00	41,44	-3,62	44	2,32
7	Up	38,00	37,19	-2,14	39	2,63
3	Down	55,00	56,37	2,50	56	1,81
5	Down	48,00	47,23	-1,60	47	-2,08

Table 2: Case $\mathcal{AE} - 4$: Pazy wing, flutter boundaries (1/2), ASWING and UM/NAST (Riso and Cesnik-2023). Comparisons with experiments (Drachinsky et al.-2022)

Flutter frequency					
AoA	Sweep type	Exp.	UM/NAST	Diff (%)	ASWING
3	Up	30,00	31,91	6,37	30,69
5	Up	29,90	31,10	4,01	30,16
7	Up	29,40	30,53	3,84	30,25
3	Down	28,20	27,77	-1,51	28,01
5	Down	26,70	27,76	3,98	28,3

Table 3: Case $\mathcal{AE} - 4$: Pazy wing, flutter boundaries (2/2), ASWING and UM/NAST (Riso and Cesnik-2023). Comparisons with experiments (Drachinsky et al.-2022)

Unloaded flutter speed						
Quantity	Unit	SOL 145	UM/NAST	Diff (%)	ASWING	Diff (%)
Flutter speed	m/s	67,30	72,40	7,58	71	5,49
Flutter frequency	Hz	34,72	34,72	0,00	33,2	-4,38
Divergence speed	m/s	100,97	98,32	-2,62	105	3,99

Table 4: Case $\mathcal{AE} - 4$: Pazy wing, unloaded flutter and divergence, ASWING and UM/NAST (Riso and Cesnik-2023). Comparisons with higher fidelity methods (Riso and Cesnik-2023)

3.5   Case AE-5-Dynamic: flutter and divergence Speed

This section introduces the evaluations of the first dynamic aeroelastic phenomena. First, a clarification must be made between flutter divergence and "regular " divergence also known as torsional divergence. The first involves the structural stiffness and inertia while the second is only the stiffness. The aerodynamic loads vary quadratically with the flight speed, there is a moment when the latter is too important to be stabilized by the structure alone. The main difference between flutter and torsional divergence is the structural behaviour. One has an exponential harmonic response (flutter) while the second an exponential only (divergence). The harmonic response is mainly due to the inertia loads of the structure. Numerically, flutter and divergence speed are usually computed through modal analysis. A flutter response involves a complex mode with a positive real part while the divergence implies a strictly positive real mode. Flutter and divergence phenomena are very dangerous are they necessarily lead to structure failure, which can be delayed by active control devices and optimal structure tailoring. Flutter and divergence speed constitute an upper bound of the aircraft flight envelope and must not be exceeded at all costs. Knowing their value is thus mandatory during the predesign process. To evaluate ASWING flutter and divergence predictions, experimental data from Dunn (1992 and 1992) have been used.

Experimental bench:
The same bench as in the steady tip deflections and twist is used. Strain gauges were fixed to the wing (cf figure 2) and connected to a numerical oscilloscope mainly to report the flutter and structural modes frequencies. The speed was incrementally increased until the flutter appeared and was reported.

Numerical bench:
The same numerical benches were used. The flutter and divergence speed analysis were conducted in 2 steps. First, a steady analysis at each flight speed must be performed in the OPER menu, so that the Jacobian matrix could be further analysed. Please refer to *section 13* of Drela (2008) for more details. Then in the MODE menu, the modal analysis were performed in order to spot the flutter and divergence modes. A first analysis was performed to have a coarse idea of the flutter and divergence speed. Secondly, the speed range was refined to precisely spot the desired intels.

Results: Each laminates modal analysis are presented in figure 5. The unstability zone has been highlighted in red. On each row, the analysis presents the modes in the complex plane, the damping factor and the frequency of the first mode in function of the flight speed.
The laminate $[0_3/90]_S$ is characterized by very close divergence and flutter speeds as highlighted by the middle figure 5-(a). The flutter response is dominated by the first torsional mode. From the frequency plot, no coalescence is clearly identified. The divergence comes from the first bending mode.
The laminate $[+15_2/0_2]_S$ clearly shows the benefit of a positive torsion/bending coupling. The flutter speed is still characterized by the first torsion mode but slightly delayed (10% higher) as depicted in figure 5-(b). The divergence speed occurs at a much higher speed around 100 m/s (3 times the flutter speed). From the complex plane damping plots, the torsion mode tends to be a "pure" divergence mode until its damping coefficients reach -1 becoming a real unstable mode.
The laminate $[-15_2/0_2]_S$, as expected shows the drawbacks of a negative bending coupling term. Divergence speed occurs before the flutter speed. It was difficult as for Dunn to clearly identify the nature of each mode, so the change in the figure 5-(b) legend. Note that the first mode was the first to lead to divergence while the third is leading to flutter later.

Experimentally it was reported by Dunn that the divergence speed of the $[+15_2/0_2]_S$ could not be detected as it was over the wind tunnel maximum speed (50 m/s). Also as $[-15_2/0_2]_S$ was reported to be extremely unstable after the divergence speed occured, the flutter speed could not be evaluated. The nature of each divergence was reported based on video recording and observation. The ASWING predictions

against experimental data were reported in Table 5 and 6. A comparison with Dunn's high-order finite element model is also presented. Overall ASWING shows excellent agreements with the experiments and better performances than Dunn's model except for the flutter frequency of the $[0_3/90]_S$ laminate. Despite the low aspect ratio of the wing considered, ASWING provides excellent results regarding the flutter and torsional divergence prediction.

Other work from the literature : Work from the literature can be invoked to robustify the conclusion on the flutter speed prediction capacity of ASWING. Variyar et al. for example did an evaluation against low aspect ratio configurations with a high sweep angle (Goland and Agard) showing similar predictions performances. Love et al. compared the ASWING and NASTRAN ("higher" fidelity) modal response and flutter speed predictions of a high aspect ratio flying wing. Again good performances were witnessed. Colas et al. presented a comparison between ASWING and NASTRAN of the flutter speed and frequency at different flying altitudes on a HALE aircraft (High Altitude Long Endurance). Excellent prediction performances were witnessed on the high-aspect configuration.

3.6   Case AE-6-Dynamic: Effect of a Nacelle/tank's relative position on the flutter speed

Nacelle and tanks can be modelled in ASWING using point masses or slender bodies. They can be rigidly attached to a wing with a pylon. The position and mass properties of a tank or nacelle can have a huge impact on the modal and aeroelastic response of a wing. To evaluate this, the experimental data provided by Runyan and Sewall-1948 were used. Note that this work has already been used in the structural part of this sequel evaluation work (Part III)

Experimental bench: The tests were performed in the Langley 4 by 5-foot (1.2 by 1.5 meters) flutter research wind tunnel. The modal response was performed in no flow condition but in the wind tunnel. A straight wing was vertically mounted from the top of the section as shown in figure 9. The wing-half aspect ratio was 6 making a good stress test for the ASWING model. The wing geometrical and structural parameters were given in the author's work and have been translated into the ASWING formalism and metric system in tab 12. The bending and torsional stiffness were determined experimentally from the static deflection curves of the wing in bending and torsion. Vibrations were recorded thanks to strain

gages placed on the wing as depicted in figure 9. The gages were connected to a system of bridges/amplifiers cascade to reduce the measurement noise. The frequency report was made on an oscillograph. In total 100 runs have been performed, to be sure that the wing did not get any structural damage from one run to another, a modal response measurement was performed before and after each one of them. In light of the results, the author reported that the wing did not witness any damage during the entire experiment. This was mainly due to the use of wires connected to the wing tip to prevent any high deflections when the wing entered into a flutter. In total 7 weights with different properties were tested but one will have a closer interest in the 7th as its spanwise and chordwise position varies. For a better reading experience, one has denoted weights I-VI the weights 7a-f of the technical note. Those weights have very close mass properties (constant) as depicted in table 11. Their index mostly indicates a change in chordwise position. The latter is given as a distance to the elastic axis denoted as d_W as depicted in figure 9(b)

Numerical bench: In light of the ASWING formalism it is not possible to model a concentrated weight as this one has a non-zero inertia tensor. To do so, one has used a potential mass dipole equally spaced from the concentrated mass centre of gravity by a distance r_W (cf figure 9(b)). The punctual mass was half the concentrated's. The distance r_w ie radius of gyration is computed to recover the concentrated mass's inertia. Their numerical values are given in the table **??**. As the weights were crafted to have a minimum aerodynamic print (symmetrical and slender), I think that using a mass dipole was the best option to virtually recover the behaviour of a concentrated mass. Being said and implemented, the modal analysis were performed following the same numerical protocol described in the previous sections.

Results:

In light of the various cases considered here, damping coefficients variation with the flight speed as presented in figure 5 will not be presented for the sake of clarity. Instead, the flutter speed and frequency of each case have been summed up in Table 7 where ASWING predictions errors are presented. The flutter speed predictions are in good agreement with experiments with a mean error of 6.9 % and a standard deviation of 5 % . The flutter frequency predictions however are not as good with a mean error of 11.6% and a standard deviation of 10%. The most important intel provided by Table 7 is that ASWING captures well the spanwise and chordwise position effect of a concentrated mass on the flutter appearance. Indeed weights that are placed forward from the elastic axis tend to delay the flutter appearance. When the weights are laterally placed between 1/3 and 2/3 of the span, the flutter speed increases no matter the
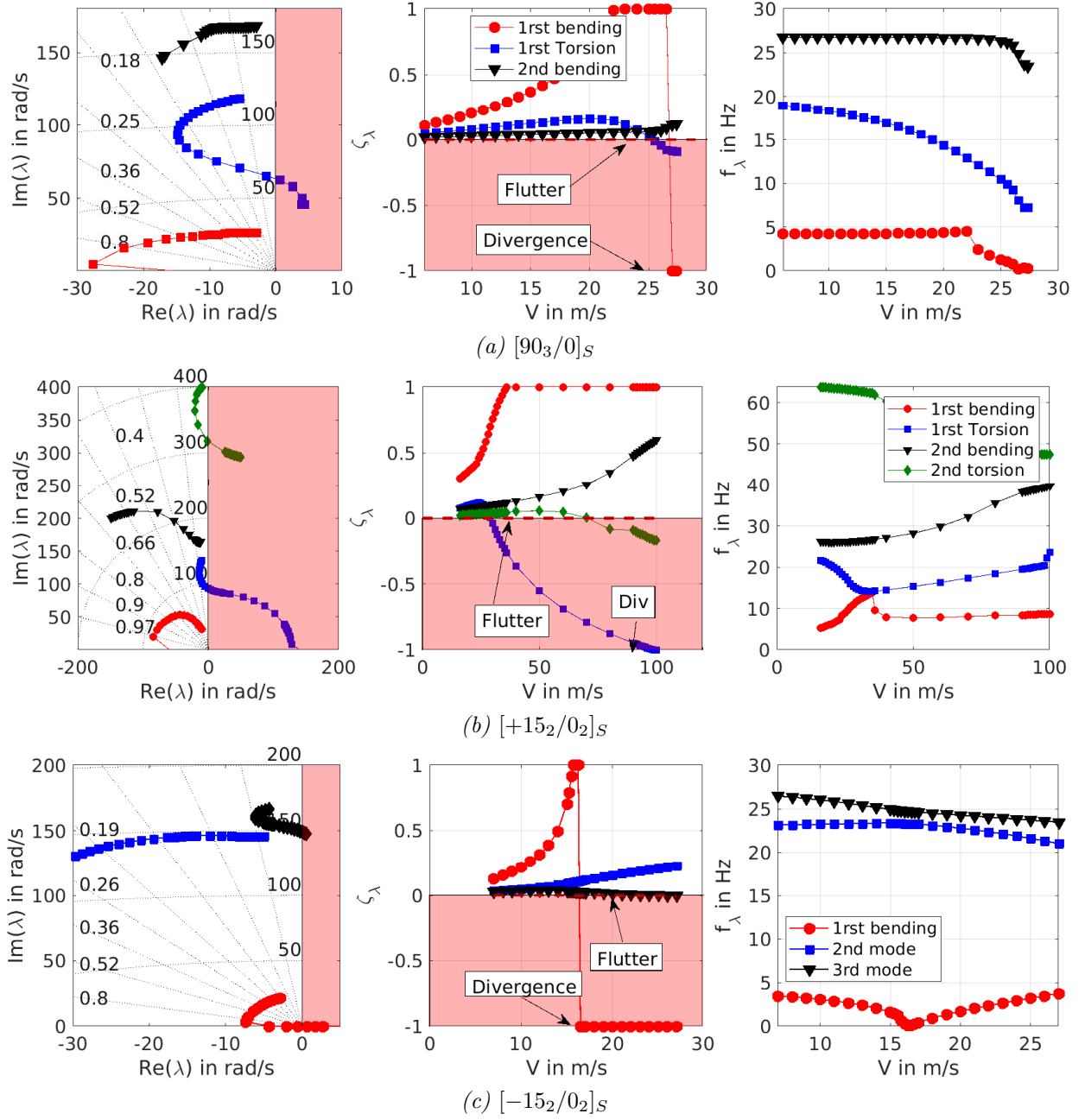
(a) $[90_3/0]_S$

(b) $[+15_2/0_2]_S$

(c) $[-15_2/0_2]_S$

Figure 8: Case $\mathcal{AE} - 5$: Modal analysis of Dunn and Dugundji's layouts. Flutter and divergence speed, modal coalescence identification

Layup	$V_{f,exp}$	$V_{f,theo}$	$V_{f,ASW}$	ϵ_1 in %	ϵ_2 in %	Remark
$[0_3/90]_S$	26.5	28.27	25.5	+6.7	-3.8	N.T.R
$[+15_2/0_2]_S$	29.0	26.9	29	-7.2	0.0	N.T.R
$[-15_2/0_2]_S$	NR	35.0	25	NC	NC	**Divergence**
Layup	$f_{f,exp}$	$f_{f,theo}$	$f_{f,ASW}$	ϵ_1	ϵ_2	**Remark**
$[0_3/90]_S$	12	11.9	9.89	-0.83	-17.58	N.T.R
$[+15_2/0_2]_S$	15.0	11.6	14.89	-22.6	-0.73	N.T.R
$[-15_2/0_2]_S$	NR	13.3	23.7	NC	NC	**Divergence**

Table 5: Case $\mathcal{AE} - 5$: Flutter speed and frequency measurements, modal analysis comparison between Dunn's results and ASWING 5.96. (N.R = not reached, N.C = not computed, N.T.R = nothing to report)

Layup	Experiments	ASWING	ϵ in %
$[0_3/90]_S$	28.20 m/s	27.0 m/s	-4.2
$[+15_2/0_2]_S$	∞ N.R m/s	96	NC
$[15_2/0_2]_S$	18.04 m/s	16.5 m/s	-8.5366

Table 6: Case $\mathcal{AE} - 5$: Torsional divergence speed predictions of the NACA0012 wing (N.R = not reached, N.C = not computed). Comparisons with Dunn's experiments

chordwise location. Both observations were captured by ASWING. Capturing the nacelle position effect on the flutter appearance is mandatory in modern applications. Especially with the rise of boundary layer ingestion devices whose some can be placed near the trailing edge of a wing (distributed propulsion). ASWING could be used to estimate more precisely the performances of those when integrated as they will impact the flutter appearance.
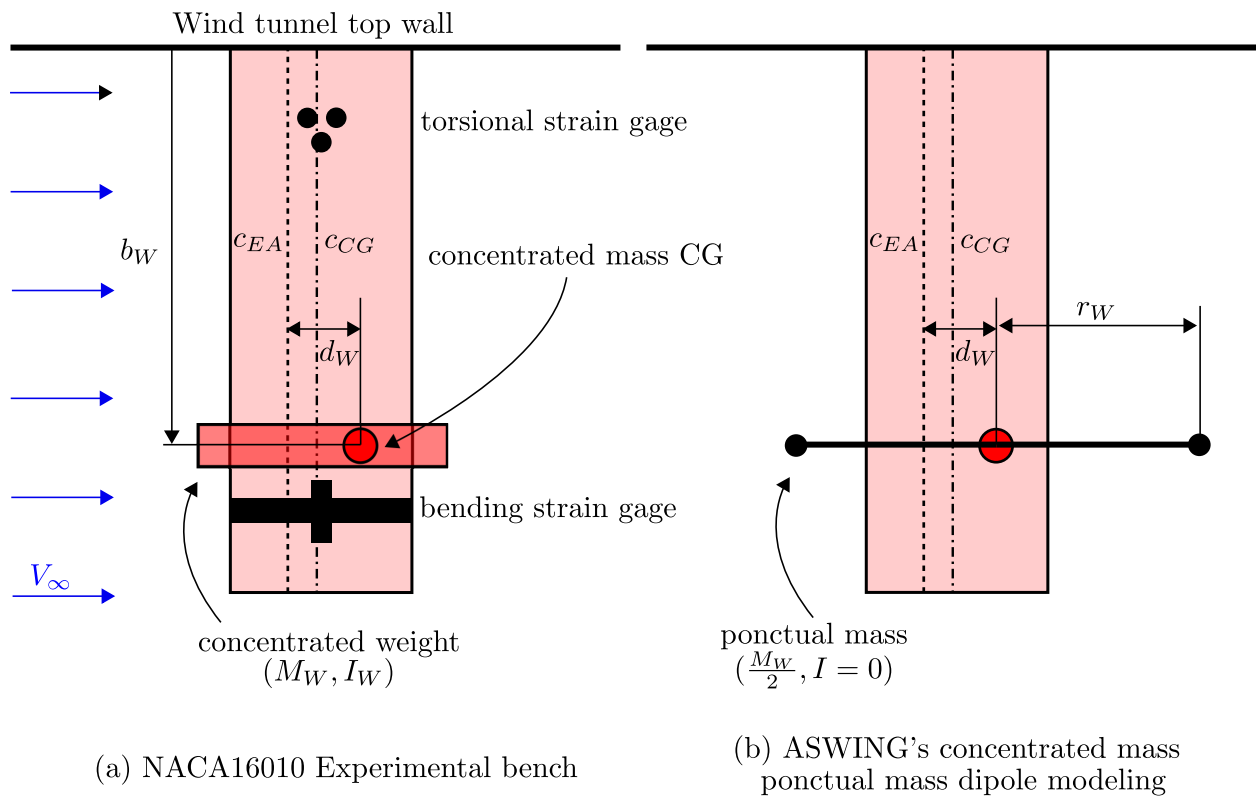
(a) NACA16010 Experimental bench

(b) ASWING's concentrated mass
ponctual mass dipole modeling

Figure 9: Case $\mathcal{AE} - 6$: Concentrated mass effect bench Runyan and Sewall (1948)

N_W	e_w	y/b	$V_{f,exp}$ (m/s)	$V_{f,ASW}$ (m/s)	ϵV_f (%)	$f_{f,exp}$ (Hz)	$f_{f,ASW}$ (Hz)	ϵ_{f_f} (%)
0	0	0	101.7	102	0.25	22.1	24.476	10.75
I	-0.818	0.17	98.6	98	-0.54	19.1	20.0	4.78
		0.23	98.8	100	1.26	17.4	18.2	4.76
		0.35	116.5	131.5	12.9	26.8	29.6037	10.4478
		0.63	160	140	-12.5	T-DIV	T-DIV	N.C
		0.94	112.2	127	3.9	T-DIV	T-DIV	N.C
I	-0.578	0.23	99.1	106	6.9	18.54	20.1	8.41
		0.44	112.776	127	12.6	24.5	T-DIV	N.C
III	-0.360	0.23	99.4	100	0.64	19.6	20.294	3.6
		0.44	105.5	126	19.4	16.5	16.1	-2.42
		0.58	111.9	137	22	14	15.6	11.42
IV	-0.140	0.23	97.5	97	-0.6	20	21.09	5.5
		0.44	96.9	102.5	5.7	17.6	18.27	3.8
		0.56	100.9	108.5	7.5	15.3	16.6	8.6
		0.69	104.6	115	10	13.2	14.9	13.2
V	0.034	0.23	95.1	93	-2.2	23.33	21.4	-8.3
		0.44	86.9	86	-1.0	17.6	19.3	9.7
		0.60	90.1	90	-0.9	14.5	16.8	15.4
		0.72	90.1	96	6.6	13	14.9	14.2
		0.83	95.7	103.5	8.1	11.4	12.9	13.3
VI	0.5	0.23	84.7	87.5	3.2	19.1	21.6	13.2
		0.33	76.8	75	-2.3	17.1	20.0	16.5
		0.5	69.8	62.5	-10.4	14.3	18.3	28.2
		0.83	74.9	68.5	-8.6	12	16.4	36.7

Table 7: Case $\mathcal{AE} - 6$: Effect of a nacelle/tank position on the flutter speed and frequency. ASWING 5.96 prediction against Runyan and Sewall's experimental data.$\bar{\epsilon V_f} = 6.9\%$, $\bar{\epsilon_{f_f}} = 11.6\%$

3.7 Case AE-7-Unsteady: Limit cycle oscillations (LCO) of a composite straight wing

This section deals with limit cycle oscillations and how ASWING can capture them. Originally introduced by Henri Poincaré in the early 20th century the LCO can have different origins in aeroelastic problems. A modal analysis as we have seen earlier is based on the linearization of the system over an equilibrium point. In the case of aero-elasticity, flutter and torsional divergence define instabilities. But most of the time, the non-linear effects are neglected in the analysis and tend to provide a small stability robustness to the system. In the case of a flutter for example, when the critical speed is reached and slightly overcome, if the system is excited it will tend to diverge but will be damped by the non-linear effect leading to a self exited oscillatory system. The more the speed is increased, the higher will be the oscillations amplitudes until the real (non-linear) divergence occurs. In the aeroelasticity problem, there are different types of non-linear terms that can lead to limit cycle oscillations. The most famous one being the non-linear structural and inertial loads ;and the dynamic stall. Other phenomena leading to LCO can be mentionned like leading edge vortices whose bandwidth can excite aeroelastic modes leading to a self excited oscillatory response. Note that the latter can happen in the stability range of the system. As ASWING is not able to capture the dynamic stall and the leading edge vortices, only non-linear structural load effects will be studied here. To do so Dunn experimental data (1992 and 1992) are used one last time.

Experimental bench:
The same bench as for the flutter boundaries section was used. The tip deflection and twist peak-to-peak amplitude were provided by two types of measuring devices that are a high-speed camera and strain gages reading. The latter were converted from empirical formulae so important error measurements were reported. During the tests, the speed was set very close to the flutter speed and incrementally increased by $\Delta V = 1.0 m/s$. A small stick pinch was applied on the wing to excite its structure (as depicted in figure 2. Dunn reported that the LCO response was extremely sensitive to the pinch intensity so great care is taken in the comment of the results. Overall they performed LCO measurements on each wing at different angles of attack. As we have seen in the previous section that ASWING is weak to predict the flutter speed when the angle of attack is increasing only the cases at $\alpha = 1.0°$ are considered. Finally, during our analysis I did not manage to get LCO on the $[-15_2/0_2]_s$ laminate, in consequence only the $[90_3/0]_S$ and $[+15_2/0_2]_S$ laminates are considered in this work.

Numerical bench:
To numerically capture the LCOs, a time marching computation was mandatory. It was not possible to implement the stick punch so a flap was used and impulsively deflected at $t = 0.1s$ as depicted in figure 10 (a). A 1° flap deflection was enough to excite the structure and reach the LCO. The time marching period Te was chosen based on a Shannon criterium on the third bending mode ($Te \approx 0.001s$). Forty structural nodes and pointwise circulation variables were enough to get a reasonable mesh convergence (please refer to the technical report Part I and III for more details). The tip deflections and twists measurements were performed using 2 numerical sensors placed at the wing tip on mid chord line. To obtain the LCO peak-to-peak amplitude, the self oscillatory response has to be established. Figure 10 (a) is depicted as the vertical displacement relative to the steady position temporal evolution. Three distinct phases can be highlighted that are the linear exponential response (red), the non-linear damping effect or LCO establishment (grey) and the established LCO (white). The peak-to-peak measurements were performed in this last zone.

Results:
For the $[0_3/90]_S$ layout, the LCO results are presented in figures 10 (b) and (c). Figure (b) present the phase average plot of the tip vertical displacement versus the tip twist variations and so for different relative speed ΔV. The latter is defined as the relative speed from the flutter one computed in the linear modal analysis. The phase average plot is provided mostly to have better insight into the flutter type and the higher frequency mode effect. For example from the shape of the plot (squeezed ellipsoïde), the effect of the second bending mode whose frequency is 2.5 times bigger than the torsional mode is clearly identified. Then the curve thickness has not been voluntarily increased, but it actually highlights the effect of higher frequency modes retained by the Shannon criterium. From the elliptic shape, it is clear that the first torsional mode dominates the limit cycle oscillations as reported by Dunn and Dugundji. Figure 10 is more of interest as it provides the ASWING and Dunn's non-linear model predictions of the peak-to-peak tip deflections and twists. The finite element model introduce in Dunn's work seems to provide better predictions at $\Delta V = 1.0 m/S$ while ASWING performed finer at $\Delta V = 2.0 m/S$. However, it is not possible to say that both show good agreement with experiments.

For the $[+15_2/0_2]_S$ layout the flutter response is much different. Indeed from the phase average shape in figure 11 (a), the coalescence of the first torsion and bending modes is clearly highlighted. Note that the coalescence was also predicted by the linear modal analysis in figure 8 (b) (frequency plot). Then the effect of the second bending mode can be identified
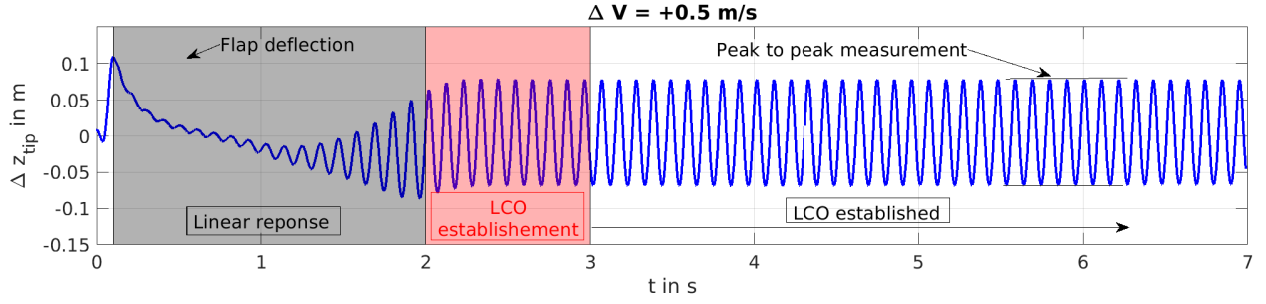
(a) Limit cycle oscillations establishment example
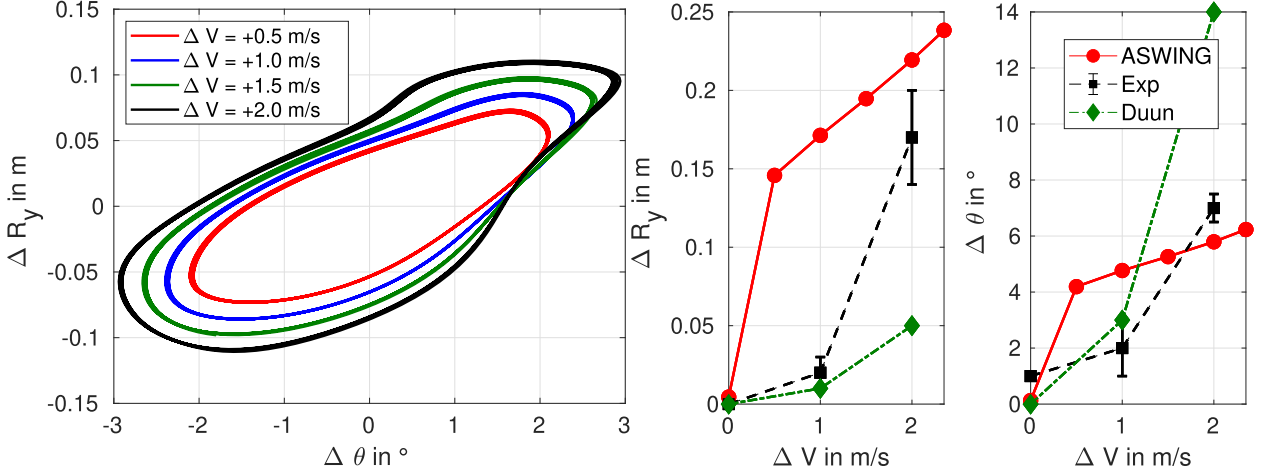
(b) Phase average evolution with flight speed above the (c) Peak to peak LCO amplitude variation with flight
    flutter speed. LCO are established   speed.

Figure 10: Case $\mathcal{AE} - 7$: Limit cycle oscillations ASWING analysis : Layout $[0_3/90]_S$. Comparison with
experiments of Dunn
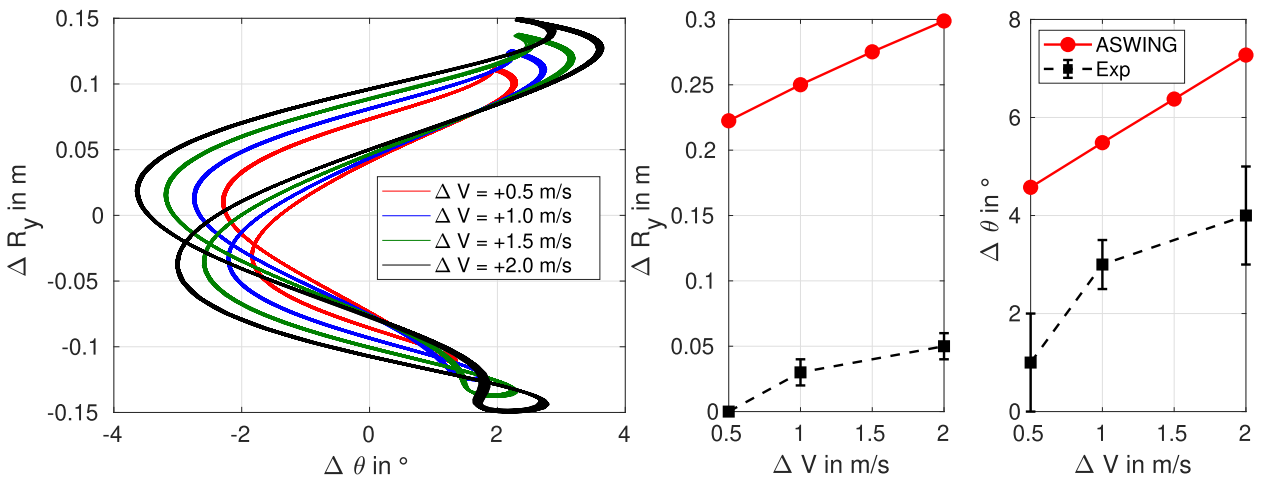
(a) Phase average evolution with flight speed above the (b) Peak to peak LCO amplitude variation with flight
    flutter speed. LCO are established   speed.

Figure 11: Case $\mathcal{AE} - 7$: Limit cycle oscillations ASWING analysis : Layout $[+15_2/0_2]_S$. Comparison with
experiments of Dunn

(small loop shape). Also as for the previous laminate, the effect of the higher frequency mode is lumped in the thickness of each plot. From the shape of the phase average plot, we can also see that the first torsion and bending modes are out of phase. Regarding peak-to-peak amplitude, Dunn's non-linear predictions are not presented as they were not clear to us. For more detail please refer to *figure 30 up and down* of his PhD script. Thus figure 11 (b) presents the ASWING peak-to-peak predictions of the tip deflection and twist against experiments. Here there is no doubt, ASWING is not able to catch correctly the amplitudes no matter the relative speed. In light of the previous results, it is clear that ASWING does not provide satisfying results regarding limit cycle oscillations. It can however capture the main tendency and which modes are dominating the LCO responses. The prediction discrepancies can come from the low aspect ratio geometry considered in this section. Thus investigations are still necessary to appreciate more precisely the capacity of ASWING to predict such phenomena. Note that during the pre-design of an aircraft, the flutter or divergence speed define an upper bound to the flight envelope not to be exceeded. So LCOs that are related to flutter and divergence are very unlikely to be encountered in real flight. Usually, aircraft manufacturers do not prioritise their studies.

It is difficult to evaluate Aswing on this type of device, as not so much experimental data exist yet. But based on the experimental evaluation already done through these technical reports, it is possible to assess Aswing performances. To do so, some of the cases of our first technical [24] report can be invoked. In particular, the two tandem cases (case $\mathcal{SA} - 7$ and $\mathcal{SA} - 8$), that showed that wake interference are correctly captured in Aswing. Also case $\mathcal{SA} - 6$ showed that Aswing correctly captures the first order flap derivatives on a lifting surface. Thus the aerodynamic of taileron will be correctly captures by Aswing. Regarding the torsional effect of the tailerons, the structural evaluation cases can be invoked, such as cases $\mathcal{SA} - 1, 2\&3$ of [25] where Aswing is shown to provide good agreement with experiment for the twist prediction due to a punctual load/moment. If the torsion moment induced by the taileron is reasonable, Aswing will capture correctly its effect in the twist distribution of the forward main wing. Finally every steady aeroelastic evaluation cases presented in this report can be mentioned to strengthen this conclusion. Despite these comments, the reader is invited to be careful with these conclusions. When experimental data on the behavior of tailerons will be released, this subsection will be replaced with a real evaluation upon them.

3.8   Steady: Effect of Tailerons

In the following subsections, some aeroelastic features not evaluated in this report author are commented, either based on other work from the literature or based on this evaluation work extrapolation. A first discussion is proposed on the capture of the effect of tailerons.
According to Sharpe et al. tailerons have been introduced to provide very high aspect ratio aircraft the following features.

- Suppresion of torsional divergence, by neutralizing the negative pitching moment inherent in airfoils desinged for high lift to drag ratio and low flight power.

- Replace ailerons for roll control by twisting the wing, via wing warping, which avoid control reversal which plagues conventional ailerons on flexible wings, regardless of the type of airfoil. The tailerons roll control effect is monotonic and does not change sign anywhere in the flight envelope. This feature leads to important weight reductions.

- Addition of pitch damping due to their long moment arm.

3.9   Dynamic: Transonic flutter

Flutter onset has been extensively evaluated through the cases $\mathcal{AE} - 4, 5, 6\&7$ but only at low speed and only for incompressible flow. When transonic flow are involved Aswing can show weakness to predict accurately the flutter onset, because it can not captured the so called transonic flutter dip whose major contributors are:

- Shock Wave Formation: As the aircraft approaches transonic speeds, shock waves form on the surface, leading to abrupt changes in pressure distribution and aerodynamic forces.

- Boundary Layer Effects: The interaction between shock waves and the boundary layer (the thin layer of air close to the aircraft surface) can cause flow separation, altering the aerodynamic characteristics in a way that promotes flutter.

that are not captured in Aswing. If the latter is considered to be used in an Overall Aircraft Design loop, the transonic flutter dip must be accurately captured as it can lead to strong penalty on the wing structure design as reported by Opgenoord et al.. An extension of the Aswing model has been recently

proposed by Opgenoord et al. and evaluated upon experimental data. It consist of placing a doublet distribution along the wing, to recover the effect of the shock wave on the flutter onset. The latter has shown good agreement with experimental data and has even been used into an OAD framework (TASOPT) to really highlight the constraint brought by this flutter dip [31]. In our work, only the 5.98 version was tested and it was not incorporating this feature yet. As the previous section, these comments will be replaced by a dedicated evaluation when a new version of Aswing will be released.

3.10   Dynamic: Whirl flutter

In this section, whirl flutter speed ASWING prediction is discussed. This phenomenon is different from classical flutter, as it is not produced by the wing but by a propeller fixed on the structure. When a propeller faces a non-axial flow because of any perturbation (gust, change in its shaft orientation etc) normal force and yawing moment are generated. If the latter is strong enough, it can deform the wing geometry. With the flight speed rising, there is a moment when the wing structure can no longer be stable and the flutter occurs. The term "whirl" is used, as when the phenomenon happens, the propeller canopy has a diverging whirl trajectory. . Tiltrotor aircraft (like in figure 12) are very subject to this type of phenomenon.

The most recent experimental work done on the

Figure 12: XV-15 (picture source : NASA)

topic has been proposed by Kambampati (2016 and 2017) and Costa (2015) Unfortunately, in their work, the authors did not provide all the necessary parameters needed to reproduce numerically the different benches. However, they have provided a comparison of their numerical model with experimental data. Or

the latter model derived from a less sophisticated but similar model as the one of ASWING. Indeed the structure model was a linear Euler Bernoulli beam theory where only chordwise and beamwise bending, and torsion are considered. It was coupled to a linear lifting line theory. Finally, to capture the perturbed loads generated by the propeller, a p-factor model was implemented. The latter differs from the ASWING model just by taking into account the drag contributions. Or for small perturbations, the latter is negligible and has been removed from the ASWING model. Considering ASWING p-factor model (*section 14* of Drela-2008) is similar to Kambampati's one. Thus in light of the previous comments, ASWING is expected to behave the same as Kambampati coupled models. The reader is nevertheless invited to read carefully the next lines. Thus Kambampati proposed in his work a comparison between its model and the experimental measurements. No matter the different benches tested, its model was able to predict correctly the damping ratio evolution with speed of the in the plane and out of the plane bending modes aswell as the torsion mode. It could also predict the whirl flutter speed with a good level of accuracy (below 10%). So far it is reasonnable to think that ASWING will provide the same forecast, however real comparison are planned in the future to really status.

3.11   Unsteady: Gust Reponse

During my literature review, no experimental work has been founded **yet** on the gust response of a flexible low-aspect wing. Thus to evaluate the ASWING capacity to predict the gust response, the work of Krengel et al. is invoked. The authors performed a comparison between ASWING and "higher fidelity" CFD data on a Boeing 737-like geometry (named MICADO). The simulations were performed at $Ma = 0.83$ ($k \approx 0.5$) with a gust having a wavelength of 100m with a turn-off pitch controller. They have provided in their work the total lift and moment prediction time marching simulations for a rigid and flexible aircraft. Their conclusions were that in both cases, ASWING catures well the maximum lift peak seen by the wing during the gust encounter (prediction error lower than 10%). The transient response is excellent on the rigid aircraft while it's a bit weaker on the flexible one. From an aircraft design point of view, the maximum lift peak is the most important quantity to be predicted. For the maximum pitching moment, the ASWING predictions are still in good agreement but not as good as the lift (prediction error between (10-20%). Also, the ASWING simulations were reported to be delayed in comparison to the higher fidelity one. The work of Krengel et al. is the only one that could be invoked.

However, care must be taken on their conclusions, as they have compared the ASWING simulations to higher fidelity for wich the accuracy is not known. Thus, wind tunnel campagn should be considered to rigouralsy assess the ASWING accuracy for gust analysis.

4 Folding wing tip devices

This last section is dedicated to folding wingtip devices. Those are treated in the aeroelastic part of this evaluation work as their behaviours are very close to a flexible structure. Wing Tip Devices (WTD) is a recent topic whose studies are mostly motivated by the reduction of commercial aircraft span as the airport taxes increase with it. The impact of such mechanisms on aircraft performances has been recently experimentally studied by Castrichini et al. (2016 2017), Cheung et al. (2017, 2018, 2020 and 2022) and Healy et al. (2022c,2022b, 2022d and 2022a). Folding wingtip devices can reduced the root bending moment when a gust is encountered. They reduced temporally the wing-span reduced the moment arm. Also they improve the rolling performances. By reducing the wingspan, they reduce the wing rolling damping phenomena. Thus Wings with folding wingtip can perform higher rolling rate. In this section,

4.1 Case FFWT-1: Longitudinal and lateral behavior of folding wing tips

In this section, the capacity of Aswing to predict the behavior of Flared Folding Wingtips is assessed. To do so the experimental bench of Healy [22, 23] has been used. In his work, he has studied, the effect of the airspeed, angle of attack and sideslip angle on the behavior of three Flared Folding Wing Tips. Each of the bench have been reproduced numerically in Aswing to assess its prediction quality.

Experimental setup:
The wing had a span of 1000 mm, a constant chord of 78 mm, untwisted shape, and a constant NACA0015 sectional profile as depicted in figure 14 (a) and (b). Regarding instrumentation, the model was equipped with an RLSRM08 encoder in both hinges, allowing fold angles to be measured. Testing was conducted in the 7ft by 5ft low-speed closed-return wind tunnel at the University of Bristol. The model was mounted to a six-component overhead balance, which, with the aid of a rear strut, could vary the angle of incidence of the model between −20 and +30 degrees and the side slip angle of the model between −/+ 50 degrees.

In Healy's work, testing was broken into three stages but only the first one is of interest in this work that is the static behaviour of FFWTs with side slip angle, speed and angle of attack.

Numerical setup:
Healy's bench has been reproduced numerically. XFOIL analysis of the NACA0015 have been performed at the wind tunnel conditions, but are not presented here. All the mandatory geometric parameters are provided in Healy's manuscript [23] (chapter 7) leading to 3 separate Aswing input files.

4.1.1 Longitudinal and lateral behaviour of untwisted Flared Folding Wing Tips

In this section, we present a comparison between Aswing predictions, and the experiments of Healy for the case of the untwisted flared folding wingtip.

Variation of the coast angle θ with the airspeed:
The first series of measure performed by Healy is the variation of the coast angle θ (illustrated in figure 14) with the airspeed. The comparison with the Aswing predictions is presented in figure 13 (a) to (c) for 3 angles of attack and 3 flare angles. Aswing shows good agreements for the configurations with the flare angles of 20 and 30 degrees. The dispersion of accuracy is due to the NACA0015 Xfoil polars, that have been computed at a single Reynolds number. For the 10 degrees flare angle case, Aswing shows good agreement only at low speed.

Variation of the coast angle with the angle of attack: Healy proposed a refinement of his measurement at a single airspeed that is 22m/s. He has provided the variation of the coast angle against the angle of attack for each flare angle case. This time for the 3 cases, Aswing shows excellent agreement with the experiments as depicted in figure 14 (a). The 10 degrees flare case shows weaker prediction at high angle of attack, but they are still reasonable.

Variation of the coast angle with the side-slip angle:
Healy has proposed to study the sensitivity of the 20 degrees flare case to cross wind flow at 22m/s. We did so in Aswing, and the comparison is reported in figure 14 (b) where it shows good agreements with experiments for side slip angle not exceeding 20 degrees. For the angle of attack of -3 degrees, Aswing shows weaker predictions.

4.1.2 Effect of the wing tip twist

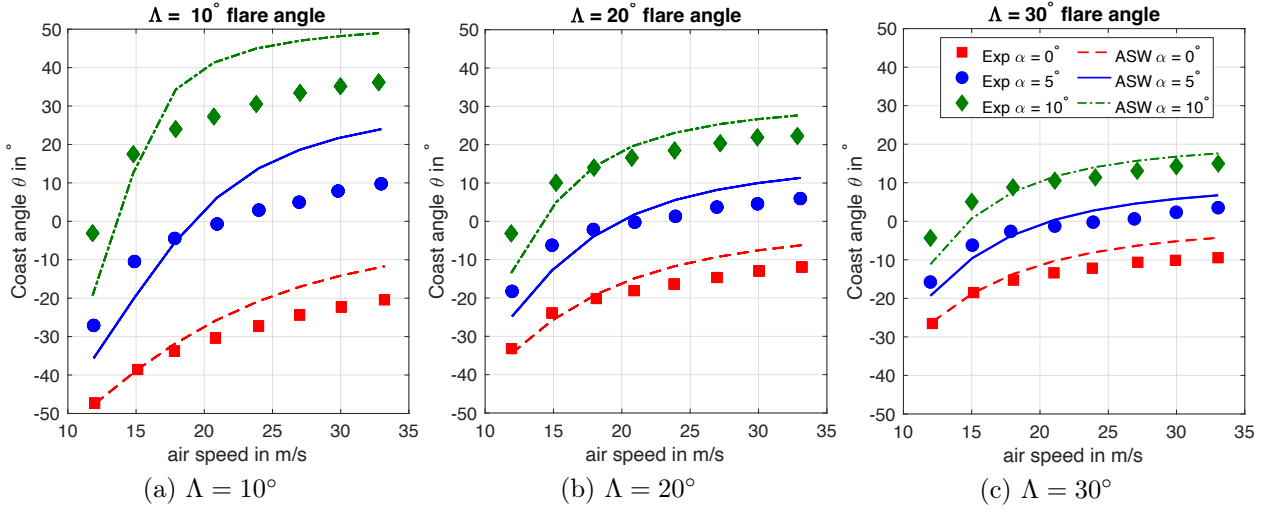Healy has extended his work, to Folding Wing Tip having tip twist variation. Indeed as for most aero-

Figure 13: Case $\mathcal{FFWT}-1$: Effect of the flare angle Λ, angle of attack and airspeed on the wingtip coast angle θ. Comparison of the Aswing predictions with the experimental data from Healy's work [22].

(a) Effect of the angle of attack at V=22 m/s

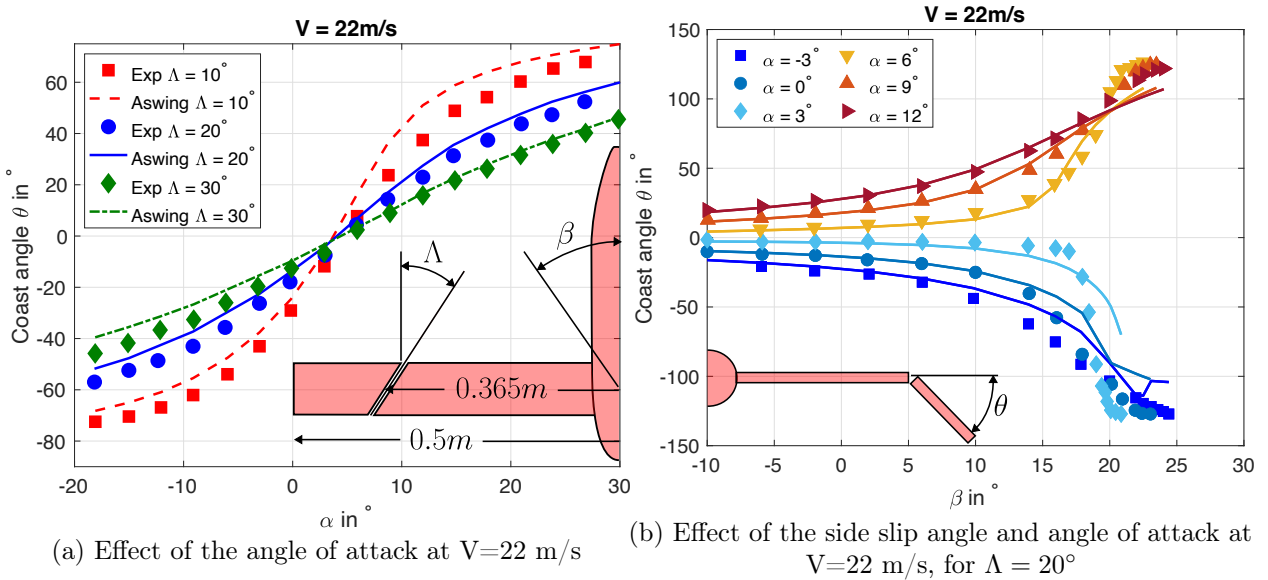(b) Effect of the side slip angle and angle of attack at V=22 m/s, for $\Lambda = 20°$

Figure 14: Case $\mathcal{FFWT}-1$: Sensitivity study of the lateral and longitudinal characteristic of Healy's bench to incidence and sideslip angles. Aswing predictions against experiments from Healy [22].

planes (such as the JWRA prototype) wingtips are usually twisted, so it is important to capture this effect. The latter is illustrated in figure 15(a). Two other benches were built having a -6 and a 9 degrees tip twist angle. Again he studied the effect of the side slip and incidence angles on the coast angle. Only the 20 degrees flare case was studied at 22m/s. Aswing predictions are compared to the experiments in figure 15 (a) and (b). In these two cases, the Aswing predictions quality decrease quite fast. We have even witnessed convergence issues for some cases, mostly due to the sharp change in the twist angle of the wingtip. However at zero sideslip angle, Aswing keep the same level of accuracy as the one of the previous subsection. In the case of this paper methodology, only the zero side slip angle is of interest, and here the level of accuracy of Aswing for every bench presented is more than satisfying.

On the real effect of Flared Folding Wing Tips: The coast angle is not really a measure, of the load alleviation provided by the Flared Folding Wing Tip. However, we have shown previously [24] that Aswing captures well the impact of various wingtip devices on the lift and drag of wings. As the root bending moment is mostly the lift integrated along the span, and by showing that Aswing captures well the variation of the coast angle with various parameters, it will captures well their effect on the root bending moment.

In conclusion, in this section we have shown that Aswing is able to capture the static behavior of Flared Folding Wing Tips with various parameters (side slip, angle of attack, speed, flare angle, tip twist). In light of the previous section, it can be used for the simultaneous analysis of joined wing with folding wingtips.

4.2   Case FFWT-2: Effect of folding wing tip on the rolling performances of a straight wing

I propose in this section to use the experimental data provided in [18] where Healy et al. studied the impact of different configurations of folding wingtip on the rolling performances of a straight wing. This time all the necessary parameters to ensure qualitative numerical analysis were provided.

Experimental bench:
A rectangular wing of aspect ratio $AR = 15$ ($b = 1.0m$ and $c = 0.067m$) was connected to a rolling rig as depicted in figure 16. An electromechanical brake could hold the wing while the ailerons are deflected. The latter spans from the wing root to $b_F = 0.364$ with a width of 25% the wing chord. Two wingtip configurations were tested. A 10 and 30-degree hinge angle Λ (cf right side of the figure 16). The hinge axis

was connected on the mid chord line at $b_H = 0.364m$. The wing airfoil was a NACA0015. In total 4 configurations were tested : *Removed* (no wing tip devices, $b = 0.788m$), *Fixed*, *Free10* and *Free30* [2]. The hinge mechanism was manufactured to be friction less. Also, the wing was designed and voluntarily re-enforced to avoid any effect from the structure. The different configurations parameters were provided by the author and reported in *Table 4* of Healy et al.'s article. Finally, the tests have been performed in the university of Bristol 7 by 5 foot low-speed closed return wind tunnel. Foour wind speed ($V = 15$, 20, 25, *and* 30 m/s) and three flap deflection ($\delta_F = 7$, 14, *and* 21°) were tested. No information on the turbulence level was provided in Healy et al.'s article .

Numerical bench:
Wing tip devices can be modelled in ASWING using joints. Their hinge axis can be specified with ease. Thus four lifting surfaces have been implemented to model the *Removed*, *Fixed*, *Free10* and *Free30* configurations. XFOIL has been used to compute the NACA0015 polars for each speed and flap deflection. A mass dipole system was used in order to reproduce the wing and folding wingtip masses and moments of inertia. The radius of gyration of the dipole was computed to find the masses positions that will recover each element's inertia.

Results:
Healy et al. performed in a first-time anchored tests. The wing was set horizontally into the wind tunnel, and the roll was prevented. Ailerons were deflected and each wingtip folding angle was measured (cf figure 16). Note that the tests were also performed with the wing upside down for the *Free10* configuration to eventually identify the manufacturing default. Figure 17 depicts the ASWING folding angles prediction against experimental data. Two markers were used for the *Free10* configuration accounting for top and upside-down tests. ASWING predicts quite well the left and right folding angles on the *Free30* configuration, especially at high speed. For the *Free10* version, the predictions are a bit weaker but still in good agreement with the experiments. Thus ASWING can correctly capture the effect of deflected ailerons on the steady behaviour of folding wing tip devices no matter their hinge angle and the flight speed.

In a second time, Healy et al. performed rolling performance measurements. Two main quantities were provided in their work that are the mean rolling rate $\bar{p}$ and the peak-to-peak roll rate amplitude Δp. Figures 18 (a) to (c) present the mean roll rate ASWING predictions against Healy et al.'s experimental data for 3 different ailerons deflections. The results are presented against the flight speed. The predictions for the *Removed* and *Fixed* are in good agreement with

---

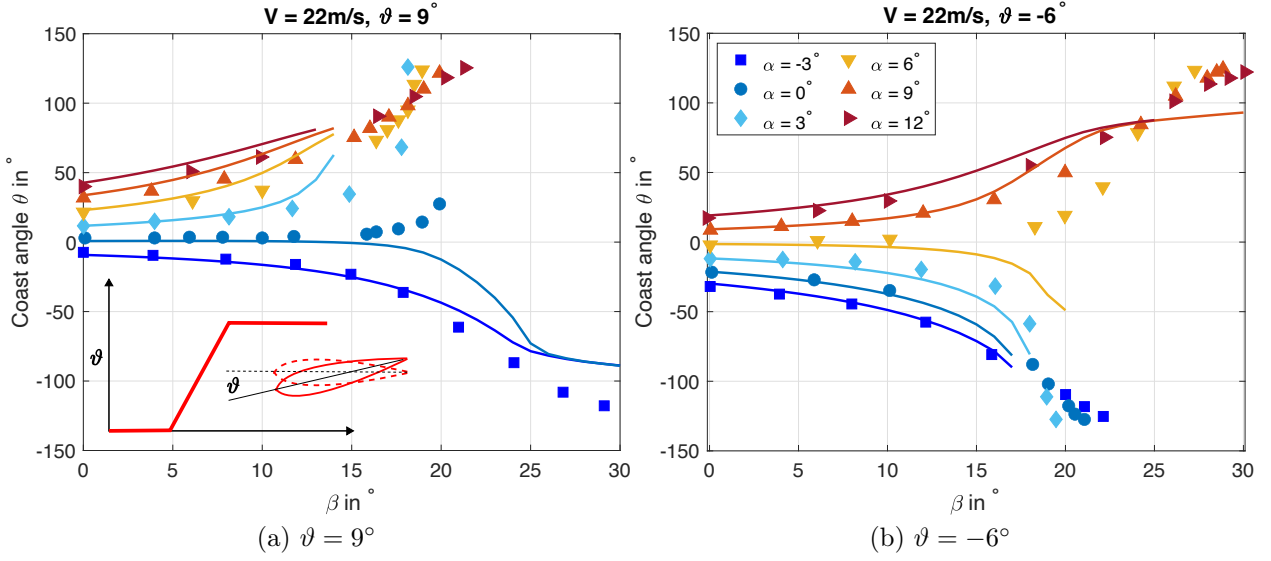[2]10 and 30 are the hinge axis angle relative to the wing cross section

Figure 15: Case $\mathcal{FFWT} - 1$: Effect of the wing-tip twist distribution on the performance of the folding wingtip. Variation with the angle of attack and side slip angle. Aswing predictions versus experiments from Healy's work [22]. Lines stops before first convergence failure.Tests were done for $\Lambda = 20°$ and V=22m/s.
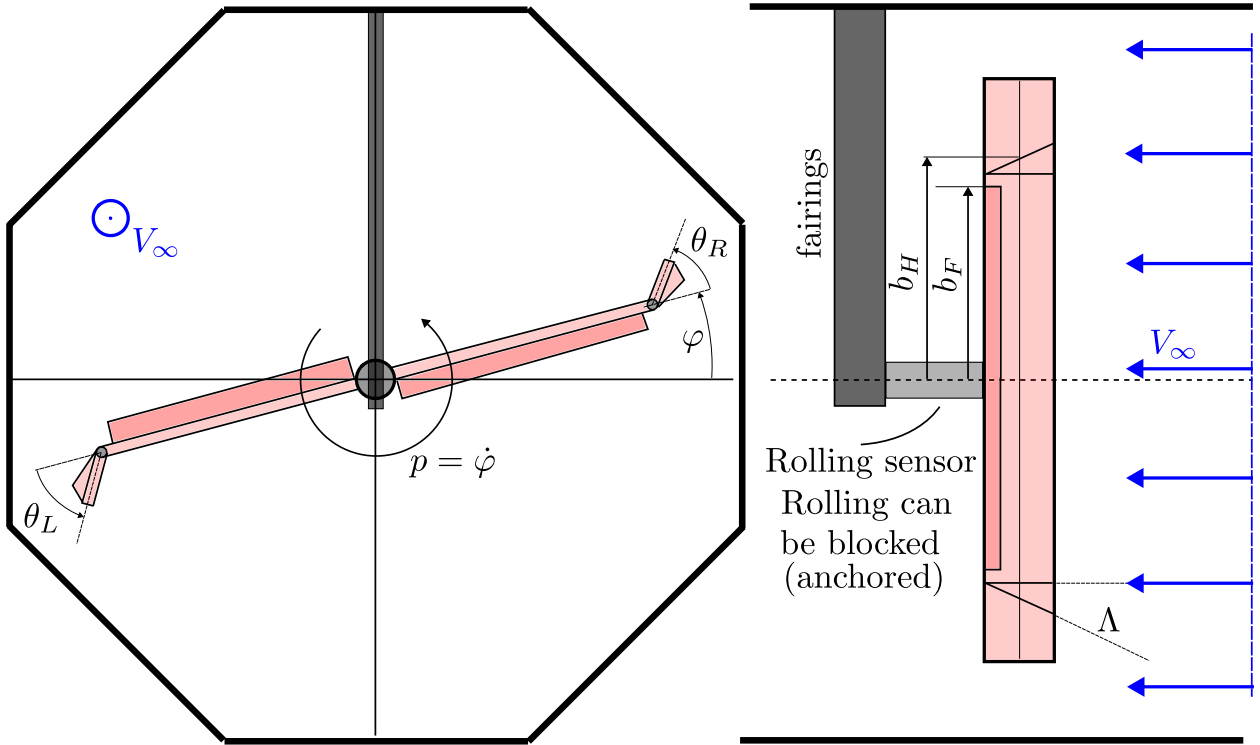

Figure 16: Case $\mathcal{FFWT} - 2$: Effect of folding wingtip on rolling performances of a wing. Experimental bench adapted from Healy et al.
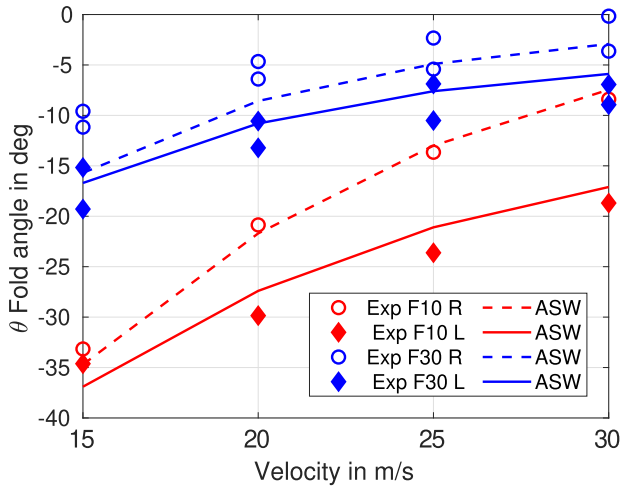
Figure 17: Case $\mathcal{FFWT} - 2$: Effect of folding wingtip on rolling performances of a wing. Experimental bench adapted from Healy et al.

the experiments which are consistent with what we have found in the aerodynamic part of this evaluation work (Part I). Even if the ASWING predictions are a bit weaker for the *Free10* and *Free30* configurations, the software correctly catches the major information. The *Free30* configuration provides better rolling performances than the *Free10* one on the complete flight speed and ailerons deflections range considered in the experiments.

Finally, because of the inertia of the wingtip devices, during the tests, when the wing was rolling the latter were also rotating around their hinge axis because of the centrifugal loads. Thus their local angle of attack was varying through time inducing an oscillation over the mean value of the roll rate. Healy et al. provided the peak-to-peak amplitude of the rolling rate and its variation with flight speed and the ailerons deflections. The figures 19 (a) and (b) depict the previously mentioned quantities and the equivalent ASWING predictions. For the *Free10* configuration, only experimental data were provided for $\delta_F = 14°$ against the speed range. For an aileron deflection of 21° the measurements were performed at a single speed ie $V = 20m/s$ (square full markers on figure 19-a). ASWING shows excellent agreement with experiments, especially at high speed. At $V = 20m/s$ ASWING loses the track and provides non-satisfying predictions. The same type of remarks can be drawn from figure 19-(b) for the *Free30* configuration. The lack of precision at low speed could come from the low Reynolds number flight where I have faced a lot of difficulties to make XFOIL converge so that to obtain the ailerons ASWING derivatives. With the flight speed increasing the problem vanished so the better predictions.

4.3   Case FFWT-3: Qualitative effect of stiff, sprung and free folding wing tip on the gust response

In this section, the experimental observations of Cheung et al. (2018) on the effect of folding wingtip on the gust load alleviation are discussed against ASWING capacity. The word "observations" is use with care as the articles Cheung et al. (2017 and 2018) has published do not provide enough information about the experimental bench to be reproduced numerically. Here, the main objective was to spot if ASWING can capture similar observations as the authors. The second one was to show the community that ASWING can model such devices.

Experimental bench:
 Two swept backward wings were placed in front of the open-jet wind tunnel at the University of Bristol. The wings span and chord were respectively 0.7 m and 0.3m. They were anchored to a plane of symmetry at the root. A balance was used to measure the total lift and root bending moment coefficient (C_L and C_l). The wing profile was a NACA0015 and was rigidly crafted to isolate strictly the behaviour of the wing tip devices. Finally, the wing tip position was chosen so that they account for a third of the exposed area. The hinge angle Λ were 10 and 30 degrees, Λ was also the wing sweep angle as depicted in figure 20. The biggest problem arise by Cheung et al.'s paper is that the author did not provide the wing tip mass and inertia. Despite the gust response introduced later is extremely sensitive to those parameters. We have chosen an estimated value in consequence but we prefer to compare observations instead of measurements. As only the latter are discussed, neither the sensors precision nor the wind tunnel level of turbulence are recalled here. In total 3 hinge stiffness were tested and provided corresponding to *Free*, *Sprung* and *Stiff* folding wingtip. Two gust vanes (cf right side of figure 20) were placed at the wind tunnel throat exit. The gust response was performed at a flight speed of 20m/s. Measurements of the lift and rolling moment coefficient were performed as well as folding angle measurements θ (cf figure 20). The upper and lower bounds in each variable change were reported against the different angles of attack.

Numerical bench:
The two benches were reproduced with ease in ASWING, except that the full wing was modelled. A numerical sensor at the wing tip was used to measure the wingtip folding angle. A mass dipole was used to reproduce the expected mass and inertia of the wing tip. The folding wingtip device and the wing were connected using a joint whose hinge axis and stiffness were specified. To reproduce the cosine gust, the inner
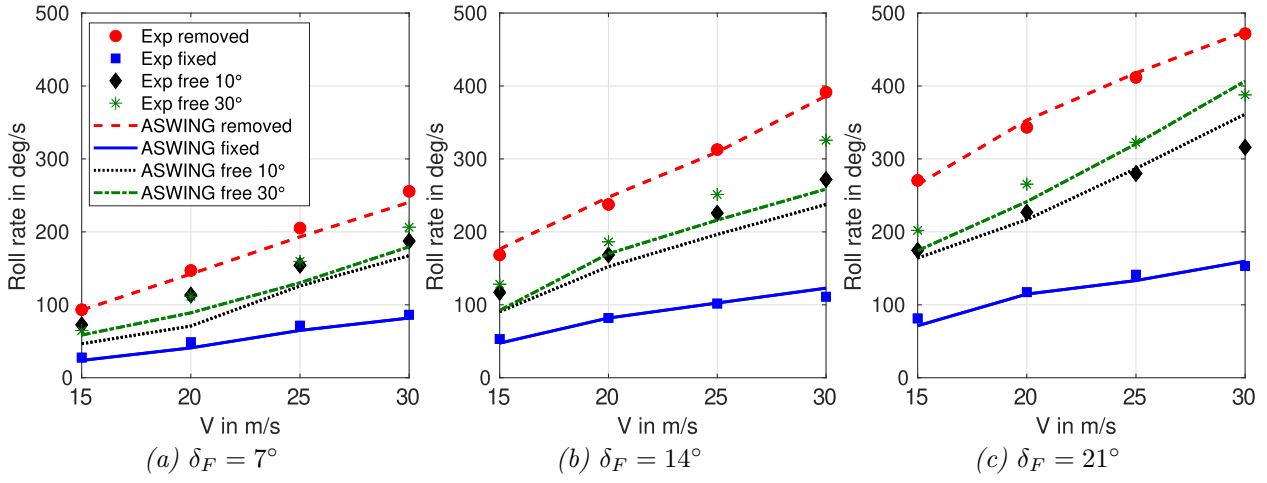
Figure 18: Case $\mathcal{FFWT} - 2$: Rolling performances of Healy et al.'s straight wing with fixed, removed and 2 free folding wing tip devices
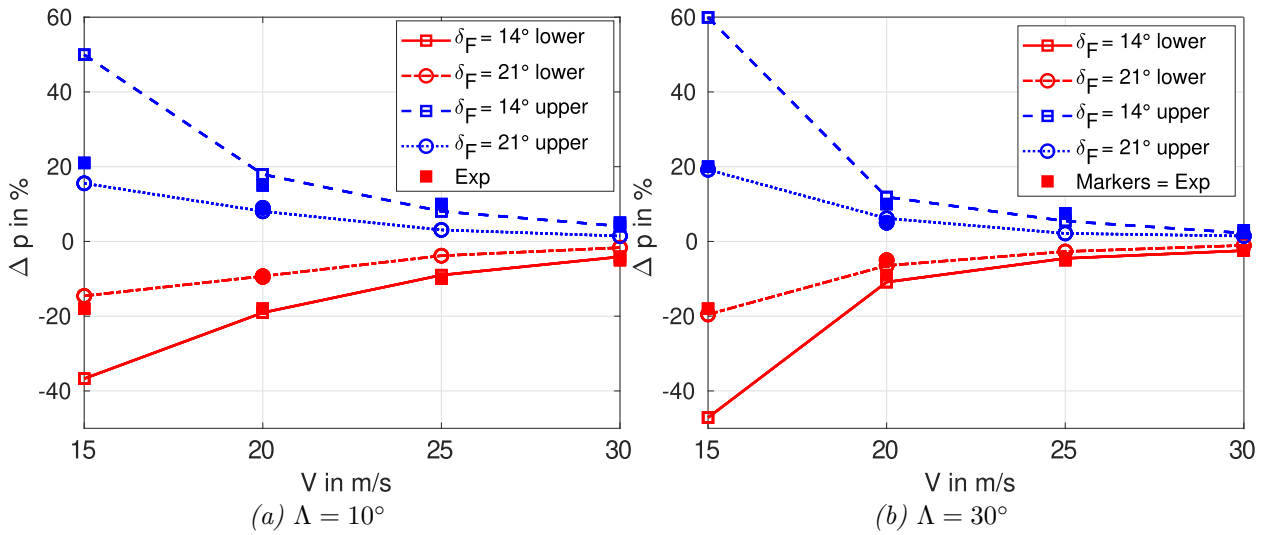

Figure 19: Case $\mathcal{FFWT} - 2$: Rolling peak to peak variation of Healy et al.'s straight wing with for various hinge angle Λ and ailerons deflections δ_F. Comparison with experiments

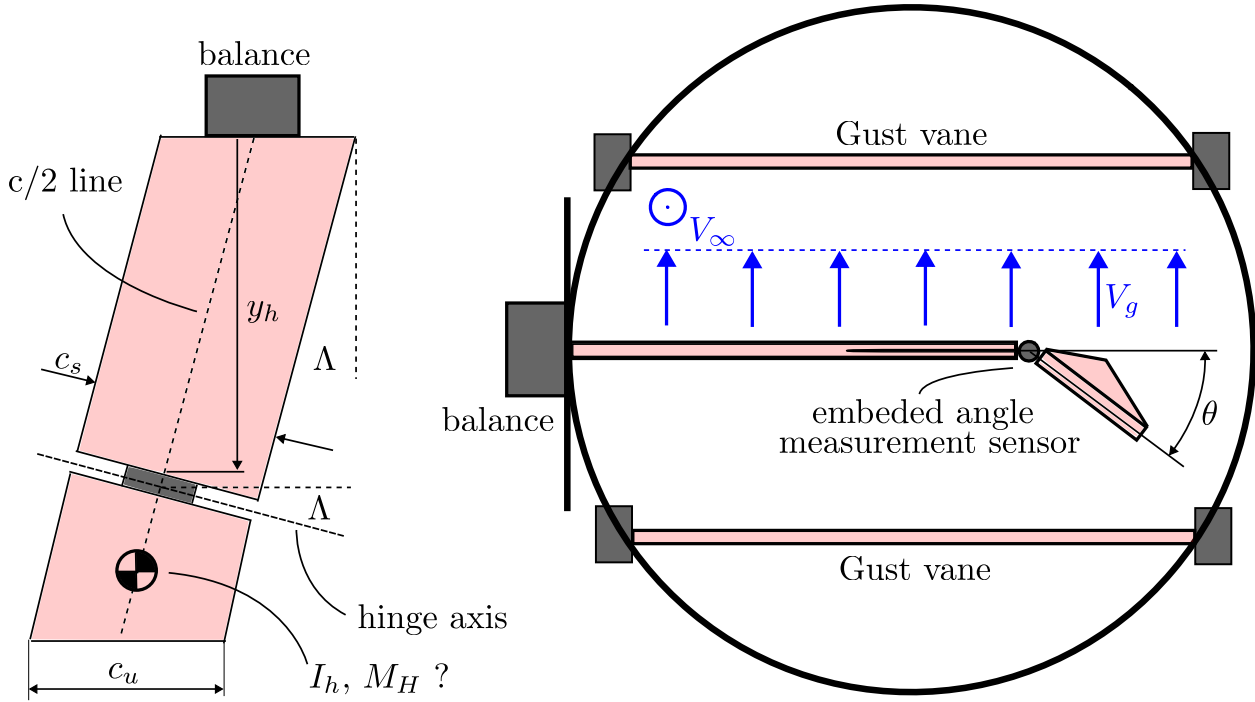Figure 20: Case $\mathcal{FFWT} - 3$: Testing of a hinged wingtip device for gust load alleviation: Cheung et al.'s bench (2017 and 2018). The gap between the wingtip and the folding devices is important leading to important pressure leaks.

ASWING gust program was used. The time marching sampling time was chosen to be 100 times lower than the gust duration. Steady analyses were also performed to investigate the wing tip aerodynamic stability on the full range of angle attack considered.

Observations:

First of all, during the steady analysis, the wingtip devices showed aerodynamic stability. In a sense that the aerodynamic loads are compensating the wingtip weight leading it to reach a stable folding angle. An so no matter the hinge angle or stiffness. The folding angle was logically increasing with the angle of attack. The same observations have been reported in the work of Cheung et al.. Secondly, figures 21 (a) to (c) are depicting respectively the upper and lower bound of the lift, rolling moment and folding angle during a gust encounter, on the $\Lambda = 10°$ configuration. The figures 22 (a) to (c) do the same for the $\Lambda = 30°$ set-up. In both configurations a significant root bending moment (rolling moment) reduction was reported on the *Free* and *Sprung* stiffness settings. They also reported that the *Free* one was outperforming slightly its stiffer version. Also, greater folding wingtip angles upper and lower were witnessed on the $\Lambda = 10°$ configuration, also observed in the ASWING simulations. In both setups, a reduction in lift coefficient during the gust encounter was reported. Overall it seems that ASWING captures well the tendency imposed by the use of folding wingtip devices on the gust response of the wing. The effect of the hinge axis angle and stiffness are also well highlighted.

4.4   Case FFWT-4: Quantitative effect of flared folding wingtips on the gust alleviation performances of a straight wing

The major drawback of case $\mathcal{FFWT} - 3$ is that, only qualitative conclusions could be drawn from it as too many parameters were missing to be able to reproduce with fidelity the benches. To robustify our observations, the work of Healy et al. (chapter 7) has been used.

Experimental bench: The same bench as case $\mathcal{FFWT} - 1$ was used so no details are recalled here. The wing with the various configurations (Fixed, Flare 10, 20 and 30) was placed in front of a gust generator. The latter was able to reproduce coarsely a cosine gust profile where the maximum gust speed and frequency could be setup with ease. The maximum vertical speeds against frequency tested experimentally are presented in figure 23 (left).

Numerical bench: In Aswing, the gust profile was spatially defined using simply the relation between gust wavelength and frequency. This hypothesis holds as the wing upcoming speed is not varying during the tests. Healy provided every structural parameters of the wing, and every weight and their inertia were converted to a set of 6 points mass systems. The time step was set up to have a same number of simulation points for every gust profile.

Results: The Aswing predictions of the maximum

(a) ΔC_L   *(b) ΔC_l*   *(c) $\Delta \theta$*

Figure 21: Case $\mathcal{FFWT} - 3$: Aswing, lift, root bending moment, and fold angle peak to peak variations prediction. Response to a cosine gust of length 7m and amplitude 0.75m/s. $\Lambda = 10°$ hinge angle. Comparison between free, sprung and stiff wingtip.

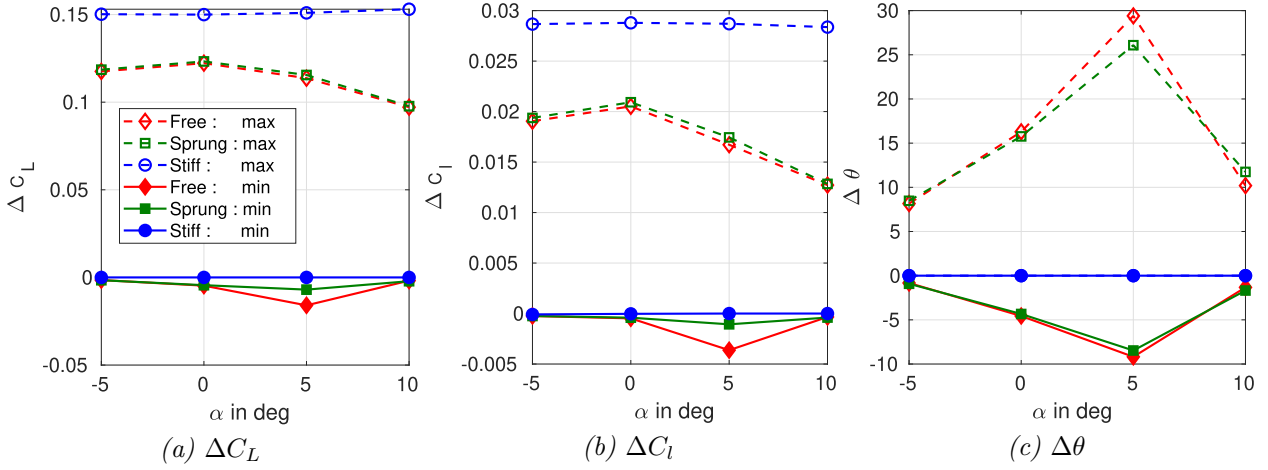*(a) ΔC_L*   *(b) ΔC_l*   *(c) $\Delta \theta$*

Figure 22: Case $\mathcal{FFWT} - 3$: Aswing, lift, root bending moment, and fold angle peak to peak variations prediction. Reponse to a cosine gust of length 7m and amplitude 0.75m/s $\Lambda = 30°$ hinge angle. Comparison between free, sprung and stiff wingtip.
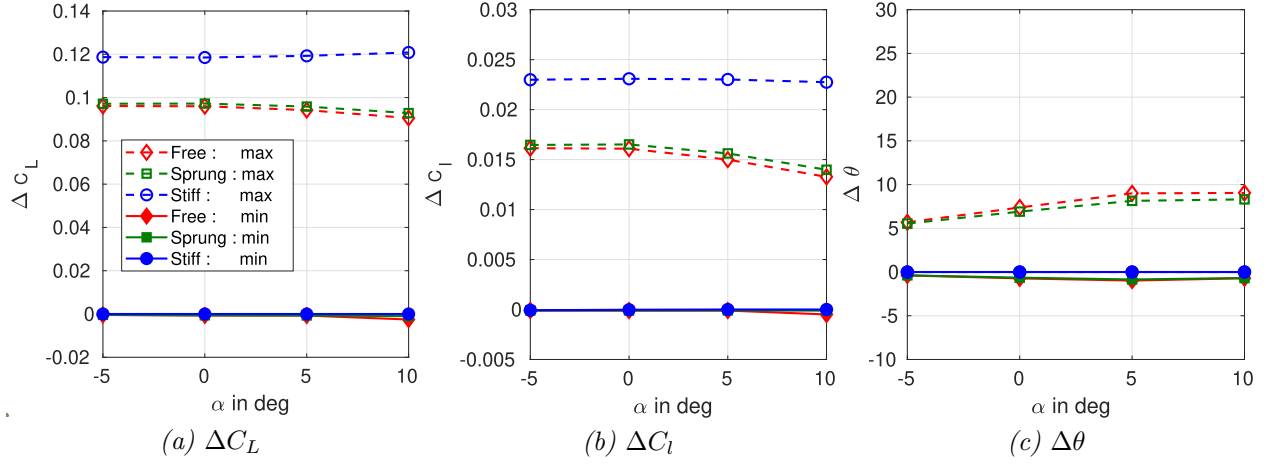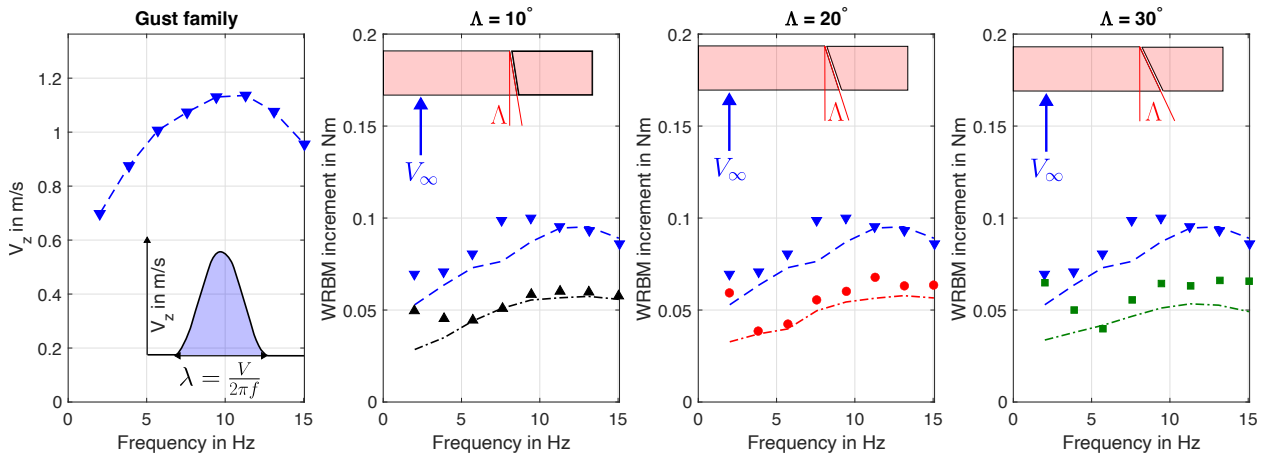

Figure 23: Case $\mathcal{FFWT} - 4$: Effect of the flared angle on the gust alleviation performance of a straight wing, on a family of gusts.

root bending moment seen by the wing with and without flared foldiing wingtips are presented 23. No matter the flare angle Aswing captures well the reduction of the root bending moment brought by flared folding wingtips, specially at high frequency. However the comparison is quite coarse. Indeed gust alleviation prediction comparison is not an easy task, as it is very difficult to reproduce perfectly the experimental condition. Indeed, as reported by Healy, first of all their wind tunnel was subject to flow distortion in steady condition (see Appendix A of [21]) leading to error in the upcoming flow condition (V_∞, α) that quantified, but such a flow field can not be prescribed yet in Aswing. Also as reported by Healy, the gust vanes do not produce a perfect cosine gust profile. The real one presents sink phases before and after the bump. Secondly the gust profile is definitely not uniform across the wind tunnel section leading to discrepancies in local free-stream velocity and angle of attack. Healy also performed numerical simulations with same level of discrepancies. As we have shown almost similar performances for the steady response in case $\mathcal{FFWT} - 1$ between Aswing and Healy model in a much more controlled environment, we believe that both models perform similarly for gust alleviation prediction, with slightly better performances for Healy model. Overall from this comparison, it is believed that Aswing will predict correctly the effect of flared folding wingtips device for gust load alleviation. We do recommend however to slightly over predict the gust alleviation capacity by 20% as a safety margin. Finally, such benches involve a lot of parameters, having a perfect knowledge of them will drastically improve Aswing predictions performances. As gust response involve the full complexity of the aerodynamic and structural model (dynamic and unsteady response), a small error in each parameter estimation can strongly affect the predictions quality.

4.5   Case FFWT-5: Effect of Flared Folding Wingtips on the flutter onset

The major advantages brought by the flared folding wingtips are to reduce the wing root bending moment during gust encounter and to provide better rolling performances. According to Gu et al., the use flared folding wingtip can lead to the design of very high aspect ratio wings. This because the gain in lift induced drag seems to out-power the gain in mass saving at iso high aspect ratio. However, rising the wing aspect ratio leads to a reduction of the flutter speed, and flutter may onset in the flight envelope. Thus, to consider using Aswing as a future aircraft design tool, it must capture the flutter speed of high aspect ratio wings

(already proven in the previous case Pazy wing) but also the detect flutter onset when the flared folding wingtips are unlocked. To this end, the experimental data from Healy et al.-2022d (chapter 5) has been used.

Experimental bench: The model (shown in chapter 5 of [21]) is a straight symmetric wing with a semi-span of 1.345m, a constant chord length of 0.15m and a constant cross section NACA0015 airfoil. The wing is split into 2 sections by a hinge located at 1 meter span. The model tip was built in 4 different versions, a fixed tip, and 2 hinge angles that are 10 and 30 degrees. The 10 degrees hinge model was built in 2 versions, one with a clean tip and another one incorporating a flap, as it was believed by Healy et al. to influence the flutter onset. The major structural loads are carried by a flat steel-plate with the dimensions of 3X25X60mm. The hinge axis was assumed to be stiffness free. The inertial properties of each beam section are provided in table 5.2 of Healy et al.'s PhD manuscript. The experiments were performed into the seven-by-five foot low-speed closed-return wind tunnel at the University of Bristol. A full detail of it can be found in appendix A of Healy et al.'s work. The flutter onset was detected at 4 angles of attack with the airspeed varying until the flutter is appearing. Two excitement methods were used to detect flutter. The first one was gust vanes while the second is a low stiffness spring released to produce a a step reponse. Both methods were producing a large band response enough to excite a low damp flutter mode. These tests were performed for each configuration of the wing with the flared folding wing tip and the tip flap.

Numerical bench: As all the mandatory parameters are provided in Healy's work, the benches could be reproduced in Aswing. To detect the flutter speed, first steady state solutions have been solved at each angle of attack and speed. For each solution a modal analysis was performed using the embedded Arnoldi algorithm. The flutter was manually detected because of numerical instabilities creating false positive cases. Care was taken to identify the same nature of the flutter mode, that is a coalescence of the FFWT flapping mode and the first Out of the Plane bending mode.

Results: Table 8 compares the predictions of Healy's model and Aswing with Healy's experiments. For the 10 degrees flare model, both framework show good predictions performances and capture the effect of the angle of attack on the flutter onset (consistent with the Pazy wing observations). For the 30 degrees flare angle, the models show both discrepancies with the experiments. Aswing shows better predictions performances at high angle of attack. The Healy's model discrepancies are due to an approximation not made in Aswing that is, "the structural model folded about a hinge line with zero flare angle. This approx-

imation significantly reduced the complexity of the equations of motion, decreasing the computational cost, and is likely a good approximation for low flare angles. However, in the case of a 30-degree flare angle, the chordwise motion of the wingtip with fold angle could likely have a significant impact on the system's dynamics". For the Aswing model, the increase of the prediction error with the angle of attack reducing is due to the flared folding wing tip working in a stall regime far beyond what Aswing is capable to capture. In consequence, for positive lift scenario (aircraft design sizing case), Aswing will provide good prediction of the effect of the flare angle on the flutter onset, that is an increase of the aerodynamic stiffness of the FFWT with the flare angle. This causes the FFWT flapping mode to have a higher frequency making it more sensitive to coalescence with the first out of the plane bending mode of the wing.

Table 9 present the Aswing and Healy's model prediction of the flutter onset for the 10 degrees flare case with the tip flap varying from -20 to 20 degrees, with normal flap convention (positive down). The tests and comparison were performed at 2.5 degrees. In these cases Healy's model shows better performances from -10 to 20 degrees. Aswing remain good at predicting the effect of the tab (flap) angle. That is a reduction of the flutter speed with a increasing flap angle. By deflecting the flap, the FFWT aerodynamic stiffness is modified in consequence. Note that with a -20 degrees deflection, it is possible the increase the flutter speed by 18%. At this point Aswing shows better performances than Healy's model to predict the flutter onset, as the FFWT is in a early post stall behaviour that is modeled in Drela's framework. From these two tables, Aswing seems to be able to capture the effect of design parameters on the flutter onset of a straight high aspect ratio wing.

On a final note, the flutter onset of the FFWT configuration were not compared to the one of the wing with fixed FFWT, because it could not be measured in the wind tunnel (out of the speed range). This, in the first place tends to show a major drawback brought by the FFWT on the flutter onset. However, the bench was built to emphasize the flutter produced by FFWT and wing mode coalescence. The aerodynamic center and elastic line are confounded so the coalescence of the torsional and bending modes could not appear. In a more representative case (swept back wing) where bending torsion couplings are involved, the conclusion could be much different.

5 Conclusions

In this report, the last part of the ASWING experimental evaluation has been presented. This part focuses on the analysis of aeroelastic phenomena. Here no theoretical reminder has been provided, the document focused on the presentation of selected experimental cases. The evaluation started with the presentation of steady aeroelastic phenomena. Deflections and twist under steady flow on a low aspect ratio wing have been presented. Three cases were studied with different stiffness coupling terms. Then, the study of the effectiveness of aerodynamic control surfaces and the reversal speed on a trapezoidal wing of low aspect ratio has been presented. Then dynamic phenomena were discussed. The same data set as for the steady deflection and twist has been used to evaluate the good prediction of the flutter and torsional divergence speed. The effect of the angle of attack on their appearance was also discussed. The various works in the literature that have reported such a validation are also recalled to consolidate the analysis. Then another set of data has been used to highlight the impact of the lateral and longitudinal position of a nacelle or an external tank on the early or delayed appearance of flutter or torsional divergence of a straight wing. A final case of flutter was discussed. In particular here, the phenomenon of flutter by precession effect or whirl flutter. A low aspect ratio wing with a nacelle/propeller anchored at its tip has been used to appreciate the good quality of ASWING prediction of the flutter speed. The report continued with a presentation of the unsteady aeroelastic phenomena. Namely the response of a structure to a vertical wind gust. Here we have failed to find experimental data, a study carried out on a commercial aircraft type 737 has been recalled. Then the steady deflection bench has been used one last time for the study of limit cycle oscillations. The LCOs being numerous and having various causes from different physical phenomena, it was question here of the effect of the non-linear structural loads bringing a light stability margin to flutter. This last case concluded the evaluation of the aeroelastic features of ASWING. However, this report has been completed by the study of folding wingtip devices with elastic hinge axis. Two experimental studies were used to assess the performance of ASWING on the prediction of the effects of these devices on the response of a wing to a vertical gust and on its rolling performance.

The different findings can be summarized as follow

- Despite bad prediction performances in the report dedicated to the structural model (Part III), ASWING captures well the steady tip deflection and twist of low aspect ratio wings. The aero-

$\Lambda = 10°$				
α	**Exp**	**ASW**	**Healy**	ϵ_{ASW} **in %**	ϵ_{Healy} **in %**
-2,5	31,7	31	32	-2,2	0,9
2,5	26,4	26	26,2	-1,5	-0,8
5,5	23	22	23,2	-4,3	0,9
8,8	20,6	21,25	20,7	3,2	0,5
$\Lambda = 30°$				
α	**Exp**	**ASW**	**Healy**	ϵ_{ASW} **in %**	ϵ_{Healy} **in %**
-2,5	19,7	14,75	15,5	-25,1	-21,3
2,5	17,3	15,25	15,06	-11,8	-12,9
5	17,2	16,5	14,93	-4,1	-13,2
7,5	17,8	17	14,69	-4,5	

Table 8: Flutter speed (in m/s) prediction of Aswing and Healy's model. Comparison with experiments. Effect of the flare angle on the flutter onset.

$\Lambda = 10°$				
δ_F	**Exp**	**ASW**	**Healy**	ϵ_{ASW} **in %**	$\epsilon_{Healy[]}$ **in %**
-20	30,65	29,5	34,4	-3,8	12,2
-10	28	28	29,03	0,0	3,7
0	25,8	26,25	26,16	1,7	1,4
10	24	25,25	24,6	5,2	2,5
20	22,5	24,5	23,7	8,9	5,3

Table 9: Flutter speed (in m/s) prediction of Aswing and Healy's model. Comparison with experiments. Effect of the flared folding wing tip flap angle on the flutter onset.

dynamic loads are distributed along the span reaching zero towards the tip. The tip pontual mass bench in the structural evaluation part involves much more important stress at the beam tip. Cross sectional shear stresses are very likey to be involved. Thus from this analysis, tip ponctual masses bench seem to not be appropriate for aeroelastic representative cases. Three different wing tailoring have been used, with various bending torsion coupling terms. All of them shows good agreements with experiments, except the case with a negative bending torsion coupling term. This feature is very important as the wing geometry of a high aspect ratio UAV is very likely to deform, specialy in thermal soaring when high load factor turn are involved. Aerodynamic performances are thus expected to vary.

- The loss of ailerons or flap effectiveness up to the reversal behaviour is correctly predicted. However, it has been shown that it can be slightly improved by taking into account the flap derivatives variation with the Reynolds number.

- The flutter speed and frequency of low aspect ratio wings is correclty captured. Also on 3 different composite layouts, ASWING predict the

nature of the divergence (torsional, or coalescence of 2 strcutral modes).

- When a nacelle or tank is anchored to a wing, the effect of its chordwise and spanwise loaction on the flutter speed, nature and frequency is well captured.

- From the litterature, it is reasonnable to think that ASWING predicts correctly the whirl flutter speed of a tiltrotor configuration. However, we invite the reader to remain carefull, as this feature has not been evaluated. Conclusions were made on litterature work involving close or similar theoretical models.

- A study of litterature has been invoked to asses the gust response predictions quality of a wing. The latter are in good agreement specificaly to compute the lift and moments peak values, which are critical parameters for structure design. However, care must be taken for gust analysis. Indeed, the unsteady aerodynamic loads are decomposed into 2 contributions in ASWING, the circulatory and added mass loads. A gust is a sudden change through time and space of the surrounding wind speed and so the air-relative one. This change is perfectly captured by the circulatory formulation but not

by the added mass term. Indeed the later is function of the inertial acceleration of the cross section mostly. The added mass terms being mostly dominant at high reduced frequencies, care must be taken when a gust is modeled to not involve such ones. Thus we recommend to study gust whose size involve reduced frequency lower than 0.2-0.5.

- Post-flutter limit cycle oscillations due to non-linear stiffening can be studied in ASWING. However the predictions show important errors with experimental measurements. Note that even higher fidelity models which have been compared, do not show better results. Also LCO is a very fundamental topic and an aircraft is very unlikely to fly in condition involving such phenomena as they are out of the safety flight enveloppe.

- Folding wingtip devices can be studied using ASWING. In this chapter, their effects on gust alleviation and rolling performances improvements have been studied and confirmed. Care must be taken on the presented results, as not all the mandatory data necessary to build the numerical bench have been provided by the author of the experimental work. However ASWING captures well the major effects brought by folding wingtip devices.

References

[1] Avin, O., Raveh, D. E., Drachinsky, A., Ben-Shmuel, Y., and Tur, M. (2022). Experimental aeroelastic benchmark of a very flexible wing. *AIAA Journal*, 60(3):1745–1768.

[2] Castrichini, A., Cooper, J. E., Wilson, T., Carrella, A., and Lemmens, Y. (2017). Nonlinear Negative Stiffness Wingtip Spring Device for Gust Loads Alleviation. *Journal of Aircraft*, 54(2):627–641.

[3] Castrichini, A., Hodigere Siddaramaiah, V., Calderon, D. E., Cooper, J. E., Wilson, T., and Lemmens, Y. (2016). Nonlinear Folding Wing Tips for Gust Loads Alleviation. *Journal of Aircraft*, 53(5):1391–1399.

[4] Cheung, R. C. M., Castrichini, A., Rezgui, D., Cooper, J. E., and Wilson, T. (2017). WIND TUNNEL TESTING OF FOLDING WING-TIP DEVICES FOR GUST LOADS ALLEVIATION.

[5] Cheung, R. C. M., Gu, H., Healy, F., Rezgui, D., and Cooper, J. E. (2022). LATERAL GUST BEHAVIOUR OF AIRCRAFT INCORPORATING FLARED FOLDING WINGTIPS. *ICAS*.

[6] Cheung, R. C. M., Rezgui, D., Cooper, J. E., and Wilson, T. (2018). Testing of a Hinged Wingtip Device for Gust Loads Alleviation. *Journal of Aircraft*, 55(5):2050–2067.

[7] Cheung, R. C. M., Rezgui, D., Cooper, J. E., and Wilson, T. (2020). Testing of Folding Wingtip for Gust Load Alleviation of Flexible High-Aspect-Ratio Wing. *Journal of Aircraft*, 57(5):876–888.

[8] Chiereghin, N., Cleaver, D., and Gursul, I. (2017). Unsteady Measurements for a Periodically Plunging Airfoil. In *55th AIAA Aerospace Sciences Meeting*, Grapevine, Texas. American Institute of Aeronautics and Astronautics.

[9] Colas, D., Roberts, N. H., and Suryakumar, V. S. (2018). HALE Multidisciplinary Design Optimization Part I: Solar-Powered Single and Multiple-Boom Aircraft. In *2018 Aviation Technology, Integration, and Operations Conference*, Atlanta, Georgia. American Institute of Aeronautics and Astronautics.

[10] Cole, H. A. (1951). EXPERIMENTAL INVESTIGATION OF ROLUNG P E RF OR MANCE OF STRAIGHT AND SWEPTBAC K FLEXIBLE WINGS WITH VARIOUS AI LERONS. *NACA Technical Note*, (2563):46.

[11] Costa, G. J. (2015). *Design, Fabrication, test, and evluation of small-scale tiltrotor whirl flutter*

wind tunnel models. Master of Science thesis, Pensylvania State University.

[12] Drachinsky, A., Avin, O., Raveh, D. E., Ben-Shmuel, Y., and Tur, M. (2022). Flutter tests of the pazy wing. *AIAA Journal*, 60(9):5414–5421.

[13] Drela, M. (2008). ASWING 5.81 Technical Description — Unsteady Extension. page 42.

[14] Drela, M. (2009). ASWING 5.86 Technical Description — Steady Formulation. page 57.

[15] Dunn, P. (1992). *NONLINEAR STALL FLUTTER of WINGS with BENDING-TORSION COUPLING*. PhD thesis, MIT, Boston, MA.

[16] Dunn, P. and Dugundji, J. (1992). Nonlinear stall flutter and divergence analysis of cantilevered graphite/epoxy wings. *AIAA Journal*, 30(1):153–162.

[17] Gu, H., Healy, F., Rezgui, D., and Cooper, J. (2023). Sizing of high-aspect-ratio wings with folding wingtips. *Journal of Aircraft*, 60(2):461–475.

[18] Healy, F., Cheung, R., Neofet, T., Lowenberg, M., Rezgui, D., Cooper, J., Castrichini, A., and Wilson, T. (2022a). Folding Wingtips for Improved Roll Performance. *Journal of Aircraft*, 59(1):15–28.

[19] Healy, F., Cheung, R., Rezgui, D., and Cooper, J. (2022b). EXPERIMENTAL ANALYSIS OF THE BEHAVIOUR OF FLARED FOLDING WINGTIPS WITH SIDESLIP ANGLE.

[20] Healy, F., Cheung, R., Rezgui, D., Cooper, J., Wilson, T., and Castrichini, A. (2022c). On the Effect of Geometric Nonlinearity on the Dynamics of Flared Folding Wingtips. *Journal of Aircraft*, pages 1–14.

[21] Healy, F., Cheung, R. C., Rezgui, D., and Cooper, J. E. (2022d). Nonlinear Stability Analysis and Experimental Exploration of Limit Cycle Oscillations with Flared Folding Wingtips. In *AIAA SCITECH 2022 Forum*, San Diego, CA & Virtual. American Institute of Aeronautics and Astronautics.

[22] Healy, F., Rezgui, D., and Cooper, J. E. (2023). Experimental effect of sideslip angle on the dynamic behaviour of flared folding wingtips. In *AIAA SCITECH 2023 Forum*, page 0376.

[23] Healy, F. J. and Healy, F. J. (2023). The impact of geometric nonlinearities on the behaviour of floating wingtips. *Aircraft Design*, 82:1–23.

[24] Jan, R. (2023a). Experimental validation of aswing. part i: Aerodynamics. Technical Report ASW-1, ISAE-Supaero.

[25] Jan, R. (2023b). Experimental validation of aswing. part iii: Structure. Technical Report ASW-3, ISAE-Supaero.

[26] Kambampati, S. (2016). OPTIMIZATION OF COMPOSITE TILTROTOR WINGS WITH EXTENSIONS AND WINGLETS.

[27] Kambampati, S. and Smith, E. C. (2017). Aeroelastic Optimization of High-Speed Tiltrotor Wings with Wing Extensions and Winglets. *Journal of Aircraft*, 54(5):1718–1727.

[28] Krengel, M. D., Hepperle, M., and Huebner, A. (2019). Aeroservoelastic Wing Sizing Using a Physics-Based Approach in Conceptual Aircraft Design. In *AIAA Aviation 2019 Forum*, Dallas, Texas. American Institute of Aeronautics and Astronautics.

[29] Love, M., Zink, P., Wieselmann, P., and Youngren, H. (2005). Body Freedom Flutter of High Aspect Ratio Flying Wings. In *46th AIAA/ASME/ASCE/AHS/ASC Structures, Structural Dynamics and Materials Conference*, Austin, Texas. American Institute of Aeronautics and Astronautics.

[30] Opgenoord, M. M., Drela, M., and Willcox, K. E. (2018). Physics-based low-order model for transonic flutter prediction. *AIAA Journal*, 56(4):1519–1531.

[31] Opgenoord, M. M., Drela, M., and Willcox, K. E. (2019). Influence of transonic flutter on the conceptual design of next-generation transport aircraft. *AIAA Journal*, 57(5):1973–1987.

[32] Riso, C. and Cesnik, C. E. (2023). Impact of low-order modeling on aeroelastic predictions for very flexible wings. *Journal of Aircraft*, 60(3):662–687.

[33] Runyan, H. L. and Sewall, J. L. (1948). Experimental investigation of the effects of concentrated weights on flutter characteristics of a straight cantilever wing. NACA Technical Note 1594, NACA, Langley Memorial Aeronautical Laboratory, Langley Field.

[34] Sharpe, P., Ulker, D., and Drela, M. (2023). Tailerons for aeroelastic stability and control of flexible wings. In *AIAA AVIATION 2023 Forum*, page 3951.

[35] Variyar, A., Economon, T. D., and Alonso, J. J. (2017). Design and Optimization of Unconventional Aircraft Configurations with Aeroelastic Constraints. In *55th AIAA Aerospace Sciences Meeting*, Grapevine, Texas. American Institute of Aeronautics and Astronautics.

Appendix - Benches properties

The table 10 provides the properties of the laminates
used for steady tip deflections, flutter and divergence
speed and LCO predictions. Data from *Appendix B
page 175* of Dunn's PhD script were used and trans-
lated to the Euler-Bernoulli formalism. Mass/length
and inertia/length were not provided and so were de-
ducted from the material properties given in *Appendix
A page 173-174* of the Dunn's work The tables 11 and
12 provide the wing and weight properties used for
the study of a nacelle position effect on the flutter
speed of a wing. The weights properties are taken
from *Table I page 8* and the wing ones are given on
page 4 of Runyan and Sewall's report. Data has been
translated from the imperial to the metric system.

Parameters	Units	$[0_3/90]_s$	$[+15_2/0]_s$	$[+15_2/0]_s$
EI_{cc}	N	1.4163	1.2947	1.2947
EI_{nn}	N	$1.8499\ 10^4$	$2.2775\ 10^4$	$2.2775\ 10^4$
EI_{cn}	N	0.0023	0.0021	0.0021
EI_{cs}	N	0	0.5151	-0.5151
GJ	N	1.2	1.2	1.4
EA	N	$1.132\ 10^7$	$1.3944\ 10^7$	$1.3944\ 10^7$
μg	kg/m	0.2310	0.2310	0.2310
$\mu g i_{cc}$	kgm	$9.2385\ 10^{-7}$	$9.2385\ 10^{-7}$	$9.2385\ 10^{-7}$
$\mu g i_{nn}$	kgm	$3.4623\ 10^{-4}$	$3.4623\ 10^{-4}$	$3.4623\ 10^{-4}$
c	m	0.140	0.140	0.140
b	m	0.558	0.558	0.558
AR	m	4	4	4
c_{EA}	m	0.5	0.5	0.5
c_{TA}	m	0.4	0.4	0.4

Table 10: Case $\mathcal{AE} - 2\&5\&7$: NACA0012 wing's stiffness and geometry parameters [15]

Parameters	M_W	d_w	$I_{W,EA}$	I_W	r_W
Unit	kg	m	kgm^2	kgm^2	m
I	1.4475	-0.0831	0.0185	0.0085	0.0766
II	1.4696	-0.0587	0.0124	0.0073	0.0707
III	1.4838	-0.0366	0.0089	0.0069	0.0680
IV	1.4933	-0.0142	0.0067	0.0064	0.0657
V	1.5059	0.0035	0.008	0.0068	0.0670
VI	1.4475	0.0508	0.0099	0.0061	0.0650

Table 11: Case $\mathcal{AE} - 6$: NACA16010 wing's concentrated weights' properties Runyan and Sewall (1948)

Parameters	c	b	AR	λ	μI_{cc}	EI_{cc}	GJ	c_{CG}	c_{EA}
Unit	m	m			kgm	kgm^2	kgm^2	m	m
Value	0.2032	1.2193	6	1	7.8E-3	41.17	20.25	0.0923	0.088

Table 12: Case $\mathcal{AE} - 6$: NACA16010 wing's geometry and structural properties Runyan and Sewall (1948)

Institut Supérieur de l'Aéronautique et de l'Espace